REPORT DOCUMENTATION PAGE

Form Approved OMB NO. 0704-0188

1. REPORT DATE (DD-MM-YYYY)	2. REPORT TYPE	3. DATES COVERED (From - To)
29-09-2014	Final Report	1-Sep-2010 - 31-Aug-2014

4. TITLE AND SUBTITLE
Final Report: Solid Mechanics: Cavitation Induced Structural and Neural Damage in Live Brain Tissue Slices: Relevance to TBI

5a. CONTRACT NUMBER
W911NF-10-1-0276

5b. GRANT NUMBER

5c. PROGRAM ELEMENT NUMBER
611102

6. AUTHORS
Ghatu Subhash,

5d. PROJECT NUMBER

5e. TASK NUMBER

5f. WORK UNIT NUMBER

7. PERFORMING ORGANIZATION NAMES AND ADDRESSES
University of Florida Office of Engineering
339 Weil Hall

Gainesville, FL 32611 -6550

8. PERFORMING ORGANIZATION REPORT NUMBER

9. SPONSORING/MONITORING AGENCY NAME(S) AND ADDRESS (ES)
U.S. Army Research Office
P.O. Box 12211
Research Triangle Park, NC 27709-2211

10. SPONSOR/MONITOR'S ACRONYM(S)
ARO

11. SPONSOR/MONITOR'S REPORT NUMBER(S)
58232-EG.20

12. DISTRIBUTION AVAILIBILITY STATEMENT
Approved for Public Release; Distribution Unlimited

13. SUPPLEMENTARY NOTES
The views, opinions and/or findings contained in this report are those of the author(s) and should not contrued as an official Department of the Army position, policy or decision, unless so designated by other documentation.

14. ABSTRACT
Cavitation-induced shock wave, as might occur in the head during exposure to blast waves, was investigated as a possible damage mechanism for soft brain tissues. A novel experimental scheme was developed to visualize and control single bubble cavitation and its collapse, and the influence of this process on a nearby tissue surrogate was investigated. The experiment utilized a Hopkinson pressure bar system which transmits a simulated blast pressure wave (with over and under pressure components) to a fluid-filled test chamber implanted with a seed gas bubble. Growth and collapse of this bubble was visually recorded during passage of the blast wave with a high speed

15. SUBJECT TERMS
Cavitation; Traumatic Brain injury; Agarose hydrogel; Shock wave, brain tissue

16. SECURITY CLASSIFICATION OF:			17. LIMITATION OF ABSTRACT	15. NUMBER OF PAGES	19a. NAME OF RESPONSIBLE PERSON
a. REPORT	b. ABSTRACT	c. THIS PAGE			Ghatu Subhash
UU	UU	UU	UU		19b. TELEPHONE NUMBER 352-392-7005

Report Title

Final Report: Solid Mechanics: Cavitation Induced Structural and Neural Damage in Live Brain Tissue Slices: Relevance to TBI

ABSTRACT

Cavitation-induced shock wave, as might occur in the head during exposure to blast waves, was investigated as a possible damage mechanism for soft brain tissues. A novel experimental scheme was developed to visualize and control single bubble cavitation and its collapse, and the influence of this process on a nearby tissue surrogate was investigated. The experiment utilized a Hopkinson pressure bar system which transmits a simulated blast pressure wave (with over and under pressure components) to a fluid-filled test chamber implanted with a seed gas bubble. Growth and collapse of this bubble was visually recorded during passage of the blast wave with a high speed camera. To investigate the potential for cavitation damage to a tissue surrogate, local changes in strain were measured in hydrogel slices placed in various configurations next to the bubble. The strain measurements were made using digital image correlation technique by monitoring the motion of material points on the tissue surrogate. In one configuration, bubble contact dynamics resulted in compression contact (>60 ?s) followed by inertially-driven tension (>140 ?s). In another configuration, the influence of local shock waves emanating from collapsed bubbles was captured. Large compressive strains (0.25 to 0.5) that were highly localized (0.18 mm2) were measured over a short time period (<24 ?s) after bubble collapse. High bubble collapse pressures 29 to 125 times that of peak blast overpressure are predicted to be the source of these localized shock waves. Consistent with theoretical predictions, these cavitation-based strains are far larger than the strains imposed by passage of the simulated blast wave alone. Finally, the value of this experimental platform to investigate the single bubble cavitation-induced damage in a biological tissue is illustrated with an example test on rat brain slices.

Enter List of papers submitted or published that acknowledge ARO support from the start of the project to the date of this printing. List the papers, including journal references, in the following categories:

(a) Papers published in peer-reviewed journals (N/A for none)

Received		Paper
08/22/2012	9.00	Sung J. Lee, Yu Hong, Michael A. King, Ghatu Subhash, Malisa Sarntinoranont, Jiwoon Kwon, David F. Moore. High-Strain-Rate Brain Injury Model Using Submerged Acute Rat Brain Tissue Slices, Journal of Neurotrauma, (01 2012): 0. doi: 10.1089/neu.2011.1772
08/31/2011	1.00	J. Sun, J. J. Flint, S. J. Lee, S. Guo, H. K. Xie, M. A. King, M. Sarntinoranont. Optically based-indentation technique for acute rat brain tissue slices and thin biomaterials, Journal of Biomedical Materials Research, (04 2011): 84. doi: 10.1002/jbm.b.31789
TOTAL:	**2**	

Number of Papers published in peer-reviewed journals:

(b) Papers published in non-peer-reviewed journals (N/A for none)

Received	Paper
08/23/2012 13.00	Sung Jin Lee, Jingjing Sun, Lei Wu, Malisa Sarntinoranont, Huikai Xie1. Refractive index measurement of acute rat brain tissue slices using optical coherence tomography, Optics Express, (01 2012): 1084. doi:

TOTAL: **1**

Number of Papers published in non peer-reviewed journals:

(c) Presentations

Subhash, G "Traumatic Brain Injury: An Engineer's Perspective", Department of Mechanical and Aerospace Engineering, North Carolina State University, Raleigh, NC Apr 19, 2012

Sarntinoranont, M. Lee, S.J., Kwon, J., Hong, Y., King, M.A., Moore, D.F., Subhash, G., "Blast-Induced Traumatic Brain Injury Model using Submerged Acute Rat Brain Tissue Slices," 2010 BMES Annual Meeting, Hartford, CT, October 12-15, 2011.

Subhash, G., "Characterization of Soft Tissue Surrogates and Brain Tissue for Development of Pressure-Deformation-Injury Maps at High Loading Rates, "California Institute of Technology, Pasadena, CA. Apr 11, 2011.

Subhash, G., "A Technique for Dynamic Deformation of Submerged Brain Tissue Slices" 2011 SEM Annual Conference & Exposition on Experimental &Applied Mechanics, Mohegan Sun, Uncasville, Connecticut, June 13-16, 2011.

Number of Presentations: 4.00

Non Peer-Reviewed Conference Proceeding publications (other than abstracts):

Received	Paper

TOTAL:

Number of Non Peer-Reviewed Conference Proceeding publications (other than abstracts):

Peer-Reviewed Conference Proceeding publications (other than abstracts):

Received		Paper
08/31/2011	3.00	Sung Jin Lee, Jingjing Sun , Michael King , Huikai Xie , Malisa Sarntinoranont1 . VISCOELASTIC PROPERTY CHANGES OF ACUTE RAT BRAIN TISSUE SLICES AS A FUNCTION OF CELL VIABILITY, ASME 2011 Summer Bioengineering Conference, Farmington, PA. 22-JUN-11, . : ,
08/31/2011	6.00	M. Sarntinoranont, S. J. Lee, J. Kwon, Y. Hong, M. A. King, D. F. Moore, G. Subhash. Blast-Induced Traumatic Brain Injury Model using Acute Rat Brain Tissue Slices, 2010 BMES Annual Meeting. 12-OCT-11, . : ,
TOTAL:		**2**

Number of Peer-Reviewed Conference Proceeding publications (other than abstracts):

(d) Manuscripts

Received		Paper
06/04/2014	15.00	Michael King, University of Florida, Pharmacology & Therapeutics, NF/SG, Veterans Affairs Medical Center,, Saranya Canchi, University of Florida, Mechanical & Aerospace Engineering, Malisa Sarntinoranont, University of Florida, Mechanical & Aerospace Engineering, Yu Hong, University of Florida, Mechanical & Aerospace Engineering, Ghatu Subhash, University of Florida, Mechanical & Aerospace Engineering, Jeremy Flint, University of Florida, Neuroscience. Cavitation Induced Structural and Neural Damage in Live Brain Tissue Slices: Relevance to TBI, Proceedings of the National Academy of Sciences(US) (to appear) (06 2014)
08/22/2012	11.00	Sung Jin Lee, Ph.D, Micheal A King, Ph.D., Jingjing Sun, Huikai Xie, Ph.D. , Ghatu Subhash, Ph.D., Malisa Sarntinoranont, Ph.D.. Measurement of Viscoelastic Properties in Multiple Anatomical Regions of Acute Rat Brain TissueSlices, Journal of the Mechanical Behavior of BiomedicalMaterials (03 2012)
08/27/2014	16.00	Michael King, Saranya Canchi, Malisa Sarntinoranont, Yu Hong, Ghatu Subhash, Jeremy Flint. Simulated blast overpressure induces specific astrocyte injury in an acute brain slice model, GLIA (08 2014)
10/01/2013	14.00	S. J. Lee, , M. A. King, J. Sun, H. K. Xie , G. Subhash , M. Sarntinoranont. Measurement of Viscoelastic Properties in Multiple 6 Anatomical Regions of Acute Rat Brain Tissue Slices, Journal of the Mechanical Behavior of Biomedical Materials (05 2013)
TOTAL:		**4**

Number of Manuscripts:

Books

Received Book

TOTAL:

Received Book Chapter

TOTAL:

Patents Submitted

Patents Awarded

Awards

'Significant Contribution Award' American Nuclear Society (ANS) - Materials Science and Technology Division (MSTD) (2014)

'Member-at-Large' Society of Experimental Mechanics Executive Board (2015-2017)
'Fellow of SEM' Society of Experimental Mechanics, for "Contributions to the field of mechanics and materials through fundamental experimental and theoretical investigations for high strain rate, multi-axial response of novel materials, including fracture under extreme environmental conditions, to increase understanding of material behavior." (2014)
'Technology Innovator Award' University of Florida (2014).
'University of Florida Research Foundation Professor' University of Florida (2013)
'Teacher/Scholar of the Year' College of Engineeirng, University of Florida (2013)
'Researcher of the Year' Mechanical and Aerospace Engineering Department, University of Florida (2011)

Graduate Students

NAME	PERCENT_SUPPORTED	Discipline
Saranya Canchi	1.00	
Yu Hong	1.00	
John Pittari	0.00	
FTE Equivalent:	**2.00**	
Total Number:	**3**	

Names of Post Doctorates

NAME	PERCENT_SUPPORTED
FTE Equivalent:	
Total Number:	

Names of Faculty Supported

NAME	PERCENT_SUPPORTED	National Academy Member
Ghatu Subhash	1.00	
Malisa Sarntinoranont	1.00	
FTE Equivalent:	**2.00**	
Total Number:	**2**	

Names of Under Graduate students supported

NAME	PERCENT_SUPPORTED
FTE Equivalent:	
Total Number:	

Student Metrics

This section only applies to graduating undergraduates supported by this agreement in this reporting period

The number of undergraduates funded by this agreement who graduated during this period: 0.00

The number of undergraduates funded by this agreement who graduated during this period with a degree in science, mathematics, engineering, or technology fields:..... 0.00

The number of undergraduates funded by your agreement who graduated during this period and will continue to pursue a graduate or Ph.D. degree in science, mathematics, engineering, or technology fields:..... 0.00

Number of graduating undergraduates who achieved a 3.5 GPA to 4.0 (4.0 max scale):..... 0.00

Number of graduating undergraduates funded by a DoD funded Center of Excellence grant for Education, Research and Engineering:..... 0.00

The number of undergraduates funded by your agreement who graduated during this period and intend to work for the Department of Defense 0.00

The number of undergraduates funded by your agreement who graduated during this period and will receive scholarships or fellowships for further studies in science, mathematics, engineering or technology fields:..... 0.00

Names of Personnel receiving masters degrees

NAME
Total Number:

Names of personnel receiving PHDs

NAME
Total Number:

Names of other research staff

NAME	PERCENT_SUPPORTED
FTE Equivalent:	
Total Number:	

Sub Contractors (DD882)

Inventions (DD882)

Scientific Progress

See Attachments

Technology Transfer

NA

Final Report

Cavitation Induced Structural and Neural Damage in Live Brain Tissue Slices: Relevance to TBI

(Proposal No. 58232EG)

Start Date: 01 October 2010

End Date: 31 Aug 2014

Ghatu Subhash, Ph.D.

Department of Mechanical & Aerospace Engineering

University of Florida, Gainesville, FL 32611

4. Statement of the Problem Studied

Research Objectives

We hypothesize that cavitation is a damage mechanism for blast induced traumatic brain injury (bTBI). A main objective of this project is to determine the conditions conducive for cavitation in cerebrospinal fluid (CSF) and corresponding tissue injury in 2-D brain slices. Initially, tissue surrogates will be used to develop the experimental technique, identify conditions for cavitation development, its collapse and associated pressures. With this knowledge, rat brain tissue will be exposed to similar conditions to develop quantitative analysis methods to relate neuronal damage to cavitation, pressure and strain history. Neural damage is assessed through new histological injury assays and mechanical property testing by indentation. With the data from applied peak pressure, rate of loading, cavitation threshold and histology, the ultimate goal is to develop "pressure -deformation- neural injury" maps for brain tissue.

Approach

MRI scans lack resolution to identify local neural damage due to shock loading. We have developed a testing device that can resolve real-time incidence of cavitation and tissue deformation in response to high rate loading in living tissues. An experimental setup to replicate a 2-D model of the brain has been developed. The model consists of a transparent test cell filled with artificial CSF and a brain (or a surrogate) slices which is subjected to high pressure rapid loading with a polymer split Hopkinson pressure bar (PSHPB). Imaging data acquired with a high- speed camera is utilized to identify cavitation initiation and collapse at sub –millisecond resolution. In addition, the recorded tissue deformation is used to create strain maps for the entire region of the brain slice. In our study, we have concentrated our efforts on damage being caused by cavitation in the hippocampus region of the bran, which is responsible for mood and memory. These studies were correlated to damage in brain tissue slices quantified using immune-histochemical assays and scanning electron microscopy.

In heterogeneous tissues such as the brain, there are limitations to using homogenous assumptions when explaining complex tissue interactions between different anatomical regions. There is a need for additional measures of spatial as well as transient variation in mechanical properties within different anatomical regions of the brain. The effect of tissue damage on changes in tissue stiffness is assessed locally in various brain regions with micro-indentation.

Significance

Blast-induced traumatic brain injury (b-TBI) is a signature injury of wars in Iraq and Afghanistan. The root-cause of b-TBI, i.e. what is "broken", in the brain during exposure to shock loading is currently unknown. While blast waves are well known to have negative pressure regions, the effect of such negative pressures on brain injury has not been previously explored. In this study, we focus on whether incident shock waves cause 'cavitation' in fluid regions surrounding the brain and subsequent neural damage in adjacent brain tissue. New injury mechanisms may result in novel mitigation strategies, e.g. protective gear, or identification of improved drug therapies specific to this injury.

5. Summary of the Most Important Results

We have developed new testing tools to study intracranial cavitation and the associated tissue damage caused by cavitation.

a. **Simulated intracranial blast wave test system:** A PSHPB test system was developed to generate a pressure wave that mimics a wave generated inside the head during a blast event, i.e. IED explosion. We were able to develop a system which can generate overpressure and underpressure components as well as isolate overpressure alone.

b. **Novel controlled cavitation test system:** Single bubble cavitation as may occur in the head during blast was reproduced using the PSHPB test system. Single bubble growth through collapse spanning over a duration of approximately 200- 600 microseconds was controlled and characterized over the short time scale of blast wave passage of around 5 milliseconds. Maximum bubble radii of 0.5-1.5 mm were generated. The ratios of overpressure to underpressure of approximately 4 to 10 times were achieved. Finally, estimated cavitation collapse pressures upto 124 MPa were achieved which correspond to around 125 times the measured overpressure of the blast wave.

c. **High resolution soft tissue response due to blast and cavitation events:** It was unequivocally observed that cavitation indeed occurs and the collapse of this bubble indeed causes significant strain in the tissue well after the bubble has collapsed. Clear evidence of significant tearing and damage has been observed in brain tissue. Deformation of tissue surrogates and brain tissue slices with passage of the blast wave and with single bubble cavitation was measured. High speed video allowed for spatial mapping of deformation and strain during blast. After the bubble collapse, maximum von-Mises strains up to 0.35 were measured in a local shock area of 0.18 mm^2.

d. **Early injury response due to blast and cavitation events:** Severe neural degeneration (50 %) was detected when compared to control tissue after exposure to high magnitude simulated blast wave. Exposure to overpressure blast wave induced two distinct types of astrocytic injury responses: (a) Astrogliosis (change of quiescent astrocytes to reactive state) and (b) Clasmatodendrosis (autophagic degeneration of astrocytic distal processes). Preliminary scanning electron microscopy analysis revealed severe damage to axons within the hippocampal region following cavitation.

e. **Brain tissue mechanical properties**: Brain tissues are super soft (G<1 kPa) and challenging to characterize. Baseline studies have been performed on tissue slices using a novel, optically-based micro-indentation test system. Viscoelastic behavior within various anatomical regions in rat brain tissue slices was measured and the range of instantaneous to equilibrium shear modulus was 3.8 to 0.54 kPa in the cerebral cortex, 1.4 to 0.27 kPa in the hippocampus and 1.0 to 0.17 kPa in the caudate/putamen.

5.1 Simulated intracranial blast wave test system

5.1.1 Test Cell Design

A transparent test cell with 4 mm test chamber thickness was designed to mimic the CSF layer in rat brain. A dynamic pressure sensor placed inside the test chamber was used to measure the pressure within the chamber during the test. The test cell incorporated designs features including rectangular geometry, see Figure 1 to support planar wave transit, and reduced fluid volume to restrict tissue displacement.

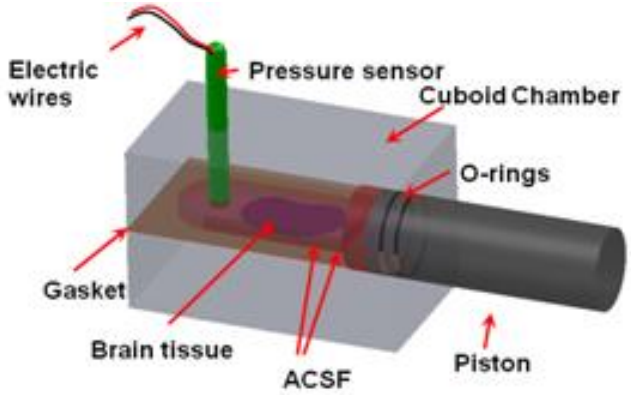

Figure 1. Schematic of the fluid filled test cell assembly with the piston rod and pressure sensor.

5.1.2 PSHPB System

Polymer split Hopkinson pressure bar (PSHPB) test system was used for generating simulated blast waves. This system is traditionally used to develop the stress-strain response of soft materials, e.g. foams, at high strain rates in the range of 500-5000/s. In this study, rather than determine constitutive response, the PSHPB device was used only to impart well-defined pressure waves to a fluid-filled specimen holder. In this way, the PSHPB device transferred momentum and high-rate loading to the test sample.

A momentum trap PSHPB was employed to create a single peak shock wave with controlled intensity. The momentum trap consists of a flange-sleeve -rigid mass assembly as shown in Figures 2 and 3 introduced at the end of the incident bar. With this trap in place the generated compression wave passes through the test cell. The reflected tension wave that starts from the stress free end of the incident bar is absorbed by the momentum trap leading to pull back from the incident bar.

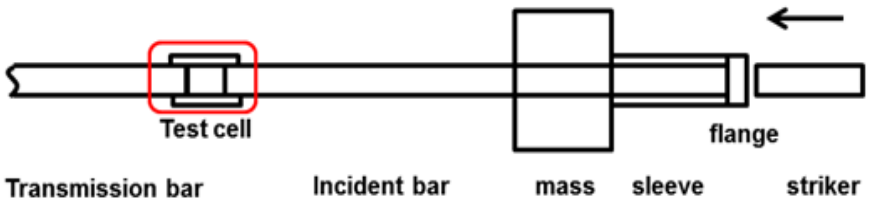

(a)

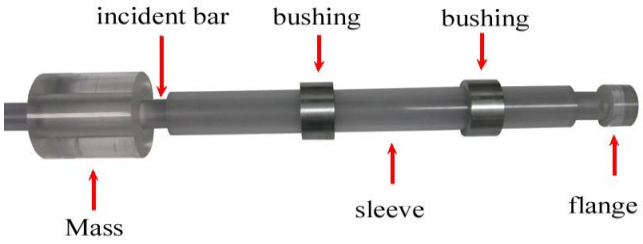

(b)

Figure 2. (a) Schematic depicting the momentum trap used in the Hopkinson bar and (b) portion of the incident bar with the momentum trap in PSHPB. The mass and the sleeve smoothly slide over the incident bar.

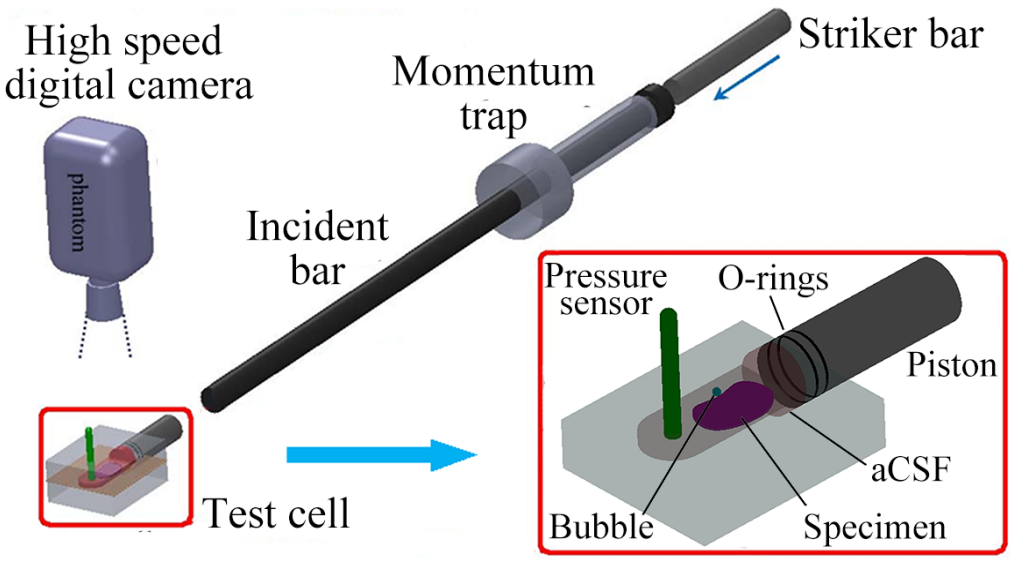

Figure 3. Momentum trap PSHPB system along with the test cell

Using the fluid filled test cell integrated with the PSHPB system as shown in Figure 3, two distinct types of blast waves were generated. The first wave had similar profile as that of an open field blast wave with both overpressure and underpressure components as shown in Figure 4(a). The other type of wave generated was characterized by overpressure component alone, see Figure 4(b). These two wave profiles allowed for identification of cavitation damage in the presence of overpressure as would occur inside the head during a realistic blast event.

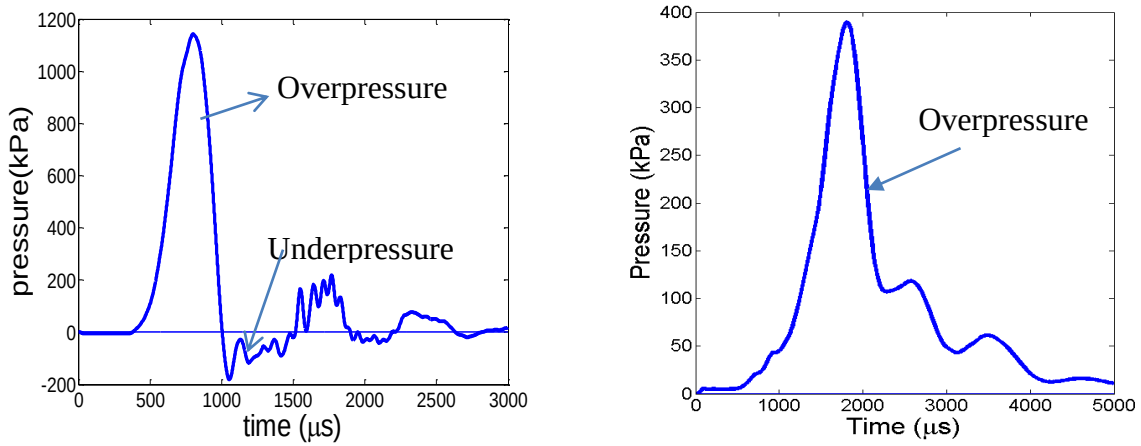

Figure 4. Typical simulated blast wave pressure profile in the fluid measured by the pressure sensor placed inside the chamber: (a) Simulated blast wave pressure profile consisting of both overpressure and under pressure components and (b) over pressure alone where no cavitation was observed in these experiments.

5.2 Novel controlled cavitation test system

For single bubble cavitation tests, the fluid-filled test chamber (Figures 1 and 3) was degassed to prevent the formation of multiple bubbles. To accomplish this, all parts of the test chamber were submerged in distilled water in a large beaker and degassed within a vacuum pump followed by soak in an ultrasonic bath to release and remove remaining small bubbles from all surfaces. A single seed bubble with a diameter of less than 50 μm was picked and placed at a predetermined location within the test cell. The temporal evolution of the bubble growth and collapse with exposure to simulated blast wave was characterized. Figure 5 illustrates a typical bubble growth and associated signal characteristics.

(a)

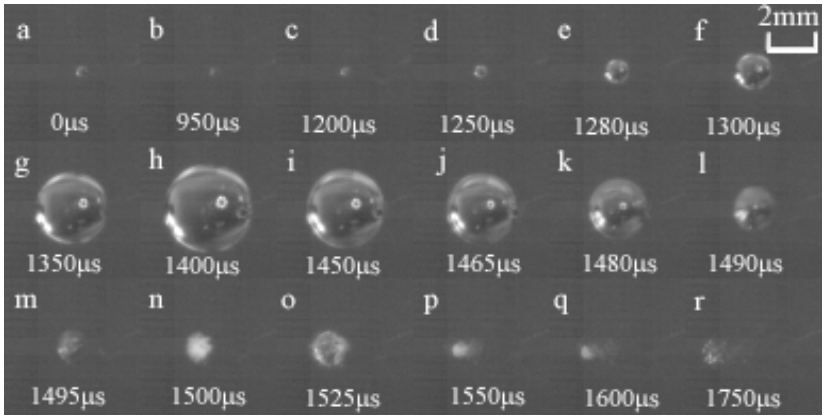

(b)

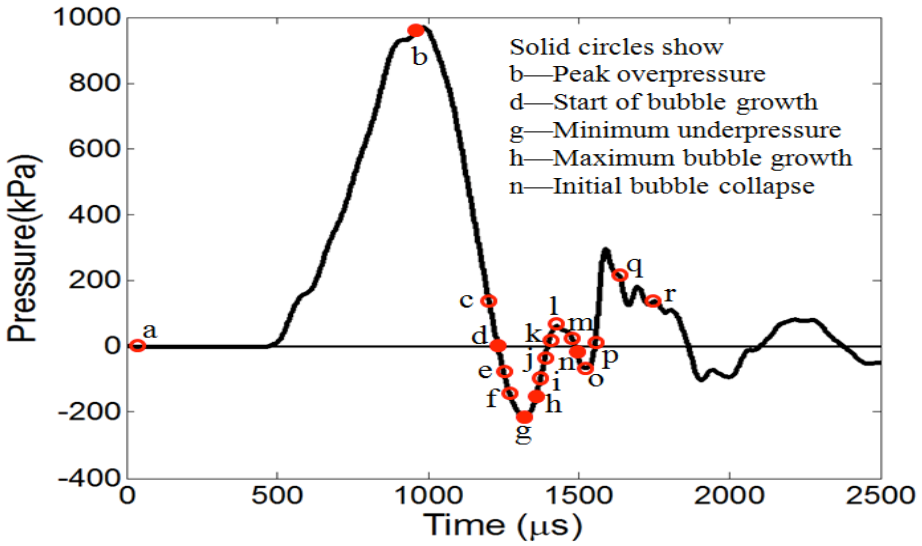

Figure 5. Dynamic behavior of a single bubble in response to a simulated blast wave. (a) Sequence of images showing evolution of a single bubble cavitation. The gas seed bubble had an initial diameter < 50 μm. (b) Corresponding pressure profile showing overpressure and underpressure phases. *t*=0 corresponds to the start of the PSHPB experiment.

The bubble remained approximately spherical throughout the test until collapse. The time from when the bubble started to grow until collapse ranged from 270 to 350 μs. The corresponding pressure profile measured within the chamber was similar to a blast shock wave with an overpressure peak phase followed immediately by a negative pressure phase and subsequent smaller oscillations. Minimum bubble size occurred at approximately the time of maximum overpressure, $P_{o\ max}$. Maximum bubble size coincided with the minimum underpressure, $P_{u\ min}$. There was a time lag (50 to 63 μs) between true minimum pressure and maximum bubble size. This delay was attributed to i) the time required for the pressure wave to travel the distance between the bubble and sensor and ii) inertial delay of bubble growth. Bubble collapse was noted at point (n) and corresponded to disintegration of the original bubble into multiple smaller bubbles.

In Figure 6, the ability to grow bubbles of various sizes and the associated pressure profiles are illustrated. Note that the maximum bubble size shown in the inset corresponds to the minimum negative pressure in the pressure profiles.

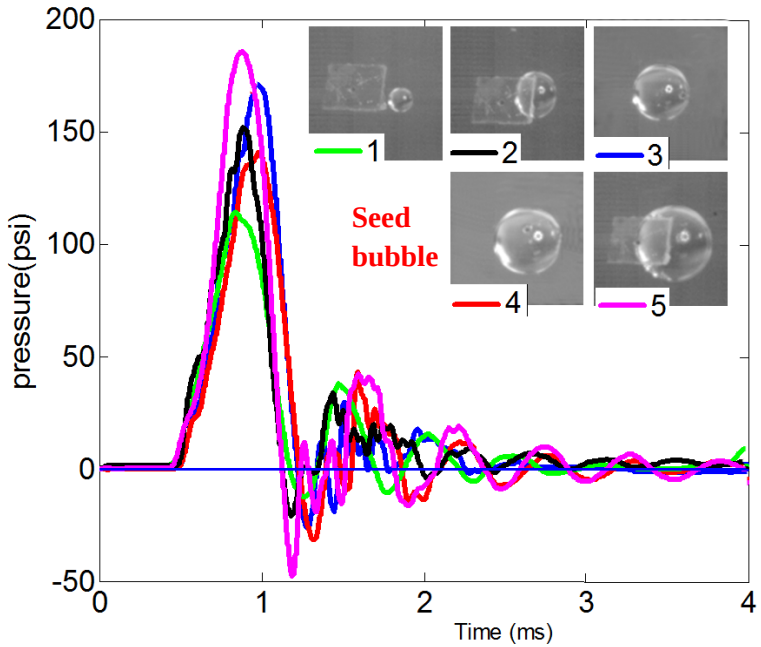

Figure 6. Pressure measured in the test chamber to control growth and collapse of a single bubble. Different PSHPB air gun launch pressures resulted in different test chamber pressure profiles and peak negative pressures. Larger negative pressure resulted in larger

bubble size. The maximum bubble sizes for each test are: 1) 0.42 mm, 2) 0.97 mm, 3) 1.14 mm, 4) 1.29 mm, and 5) 1.47 mm as shown in the inset micrographs.

Upon bubble collapse, a high-pressure pulse is released. Emission of a shock wave from a collapsing bubble has been well known since the famous theoretical work of Rayleigh (1917) on an imploding spherical cavity. The differential equation relating pressure and the radius of an isolated spherical bubble in an infinite, incompressible liquid is given by

$$R\ddot{R} + \frac{3}{2}\dot{R}^2 = \frac{P_R - P_\infty}{\rho}$$

Where, R is the instantaneous bubble radius, which can be measured from cavitation bubble images captured by the high speed digital camera, P_∞ is the environmental pressure (far-field pressure) measured by the pressure transducer placed in the test chamber, and P_R is the pressure in the liquid at the boundary of the bubble.

The measurable bubble collapse radius varied between 0.2 to 0.5 mm. It should be noted that bubble radius at collapse was difficult to determine as the bubble size approached the limit of image resolution. Therefore, it was not possible to identify the pressure at the exact time of collapse of the bubble from the images. To overcome this limitation, we have plotted the instantaneous bubble radius R during its growth and collapse as shown in Figure 7(a). A fifth-order polynomial was fit to this data from which one can calculate the corresponding $\dot{R}(t)$ and $\ddot{R}(t)$ functions and then determine the boundary pressure P_c in the fluid for each bubble radius based on Rayleigh-Plesset relation as shown in Fig. 7(b). Because the radius at the instance of bubble collapse (i.e., at R=0) is unknown we fit an exponential curve ($P_c = ke^{-R}$) for this data. The curve-fit equations for the growth and collapse of three typical bubble sizes are shown Figure 7(b). By setting R=0, we can now determine the elusive collapse pressure P_c at the time of bubble collapse i.e., P_c=k.

Typical collapse pressure for a large size bubble (i.e., large negative or tensile pressures) can be as high as 100 MPa, see Table 1. For comparison, note from Fig.5(b) that a typical value of incident blast overpressure in our set up is only around 1 MPa and the blast under pressure is around 250 kPa. Thus the local pressure at the time of bubble collapse can be as high as 100 times the incident over pressure or around 400 times the blast under pressure. These large pressures can cause severe damage in the localized regions of the brain tissue. Table 1 summarizes series of tests performed and relevant blast pressures.

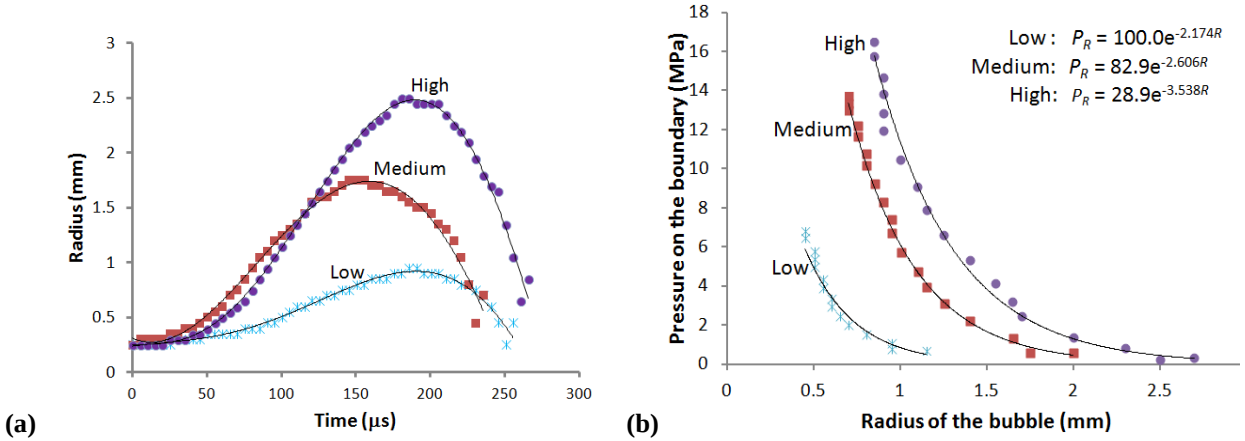

Figure 7. Bubble growth time history and calculated collapse pressure. (a) Typical bubble growth and collapse during testing. Radial profiles for three bubbles corresponding to low, medium and high underpressure groups are shown. 5th order polynomials were fit to experimental data. (b) Collapse pressure estimation method. Bubble pressure was calculated at each bubble radius for the low, medium and high underpressure tests shown in (a). Exponential equations were fit and pressure at r=0 was estimated to be the bubble collapse pressure, P_c.

Table 1. Summary of test parameters and bubble behavior during single bubble cavitation tests.

Underpressure group (sample size)	**Low (n=10)**	**Medium (n= 8)**	**High (n=9)**
$P_{u\ min}$ (kPa)	-86±11	-166±39	-315±21
Air gun pressure (kPa)	69	130	207
$P_{o\ max}$ (kPa)	851±49	943±71	1178±22
Over/underpressure duration* (µs)	586±23/157±14	643±31/168±22	723±24/184±13
Lag time† (µs)	53±2	58±7	60±3
Maximum radius of bubble (mm)	0.47±0.12	1.08±0.15	1.45±0.11
Collapse radius (mm)	0.21±0.11	0.24±0.13	0.23±0.09
P_∞ at collapse‡ (kPa)	6.51±3.32	3.38±7.44	0.51±4.65

P_c (10^3 kPa)	25.1±4.2	68.6±5.3	123.9 ±10.2
$P_c / P_{o\ max}$	~29.5	~72.7	~125.2

* Initial phases † Between $P_{u\ min}$ and maximum bubble radius
‡ Chamber pressure measured away from the bubble

5.3 High resolution soft tissue response due to blast and cavitation events

5.3.1 Hydrogel deformation: High pressure cavitation testing

Initial gel studies were conducted at high blast pressures on tissue surrogates. Figure 8 shows bubble initiation (b) and growth (c & d) near a gel edge in a degassed test chamber. These experiments showed clear evidence of shock wave generation with bubble collapse (f) that resulted in hydrogel indentation (g-i) well after the bubble has collapsed.

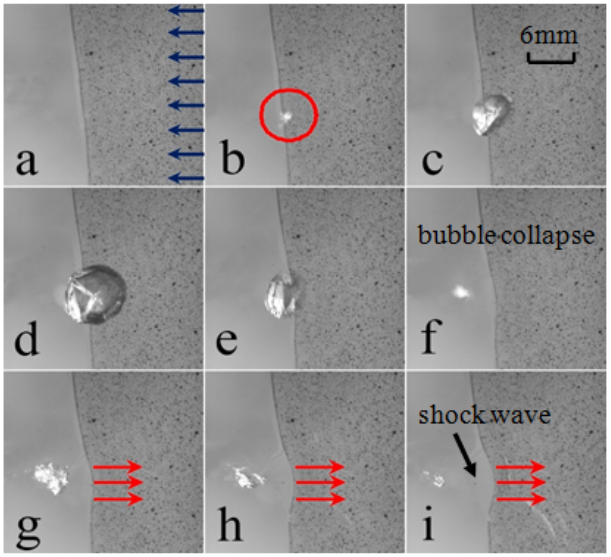

Figure 8. Bulk cavitation and tracking of a single bubble near a ballistic-gel edge. Figure (a) shows the incident blast wave direction traveling from right to left (blue arrows), (b) bubble initiation (circled), (c&d) growth, (f) collapse, and the effect on an adjacent gel slice (f-i). A local shock wave following bubble collapse resulted in highly localized hydrogel deformation (red arrows). $P_{o\ max}$ =2800 kPa and $P_{u\ min}$=-380 kPa.

5.3.2 Single bubble cavitation on hydrogels

Intent of the following types of tests is to measure the deformation fields when a controlled isolated bubble is allowed to grow and collapse in the vicinity of a hydrogel. By observing the deformation pattern utilizing the high speed imaging system, one can experimentally measure the strains during bubble growth and well after bubble collapse (shock wave generation) has occurred.

Testing was conducted on a tissue phantom, speckled hydrogel slices. The test chamber was filled with distilled water, and a 1 mm thick hydrogel slice was placed on bottom of the test cell. It should be noted that the piston used to impart the pressure wave was in contact only with water in the test cell, not the hydrogel slices, throughout testing. For follow-up strain mapping, hydrogel slices were speckled with black stamp ink (AccuStamp, Cosco Inc) using an air brush. Methodology for the introduction and control of a single bubble was followed which included degassing with vacuum pump, followed by soak in ultrasonic bath and introduction of seed bubble at predetermined location. Next, the hydrogel slice was moved a fixed distance (0.5 mm) from the seed bubble (~0.05-0.1 mm diameter). Once the piston impacts the incident bar, the induced pressure wave caused the seed bubble to grow and collapse. Corresponding deformation of adjacent hydrogel was recorded with our high speed camera (60,000 frames per second), see Figure 10. The cavitation induced damage was assessed at two locations by controlling the placement of the bubble with respect to the slice; (i) bubble placed at the edge of the slice (Figure 9) (ii) bubble placed underneath the slice (Figure 10).

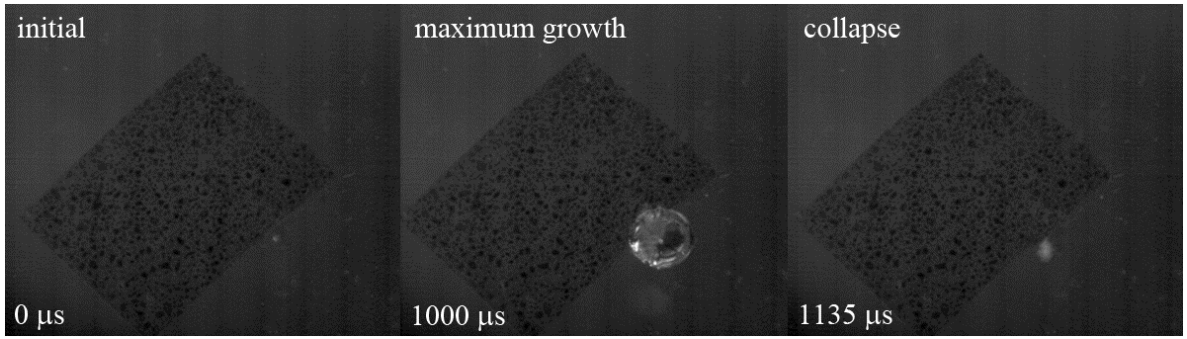

Figure 9. Speckled hydrogel slice deformed during single bubble growth and cavitation near the edge of the slice.

5.3.2.1 Hydrogel deformation: Single bubble at an edge

Using digital image correlation (DIC) and a series of high speed images, we calculated displacement of every speckle in the gel as well as the principle strains at each point, see Figure 10. Figure 11 shows the bubble radius during its growth and the associated principle strains for the nearest point in the hydrogel. Principal strains reached a peak value when the bubble grew to the maximum size and after the bubble collapse the gel retracted back to its original position and then due to inertia continued to move in the same direction causing another peak as seen in the Figure 11. The full field strain map calculated using DIC for the hydrogel revealed that the maximum strain occurred at material points which were in close contact with the bubble during its expansion and contraction phases.

As the bubble grew, the hydrogel edge was deformed by direct contact with the expanding bubble. Radial strain (ε_{rr}), circumferential strain ($\varepsilon_{\theta\theta}$) and von Mises strain ($\varepsilon_{VM}$) are shown in Figure 10. It should be noted that deformation and strain fields were not calculated in regions where the bubble overlapped the edge of the hydrogel (masked regions) since there was distortion of the observed speckle field due to the overlapping bubble. As these regions experience maximum strain, the values close to the edge could not be calculated. Overall, large deformations were captured and magnitude of calculated strains decreased with distance from the bubble center.

The effect of local shock wave generation following bubble collapse was not seen by changes in ε_{rr} for this bubble configuration (no compressive strains after bubble collapse). This was because either the edge of the hydrogel was not sufficiently close to the center of the bubble to sense the shock wave, or the expanding bubble pushed the entire hydrogel slice away from the bubble rather than inducing local deformation.

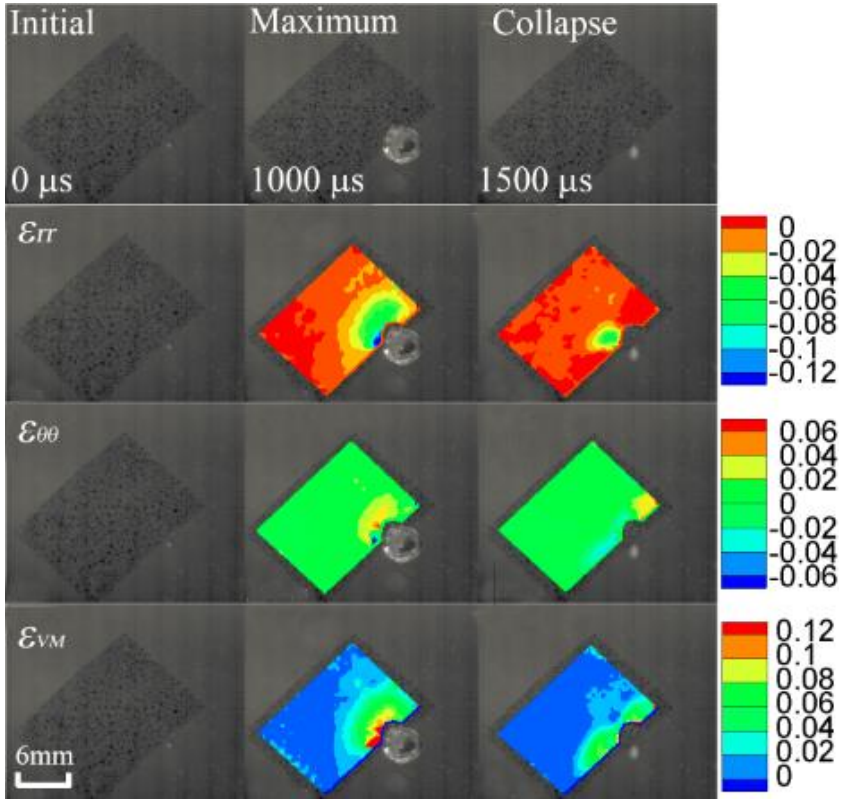

Figure 10. Single bubble cavitation at the edge of an agarose hydrogel slice. (Top row) High speed images showing initial seed bubble at edge, maximum growth and collapse at selected times; (2nd row) radial strain, (3rd row) circumferential strain and (4th row) von Mises strain at the same time points. Regions at the edge were excluded due to masking by the impinging bubble. Test chamber was degassed before gas seed bubble (< 50 μm diameter) was placed to the side of the hydrogel (~1 mm gap distance). t=0 corresponds to the start of the PSHPB experiment. Simulated blast wave traveled from right to left with $P_{o\ max}$ =1260 kPa and $P_{u\ min}$=-189 kPa.

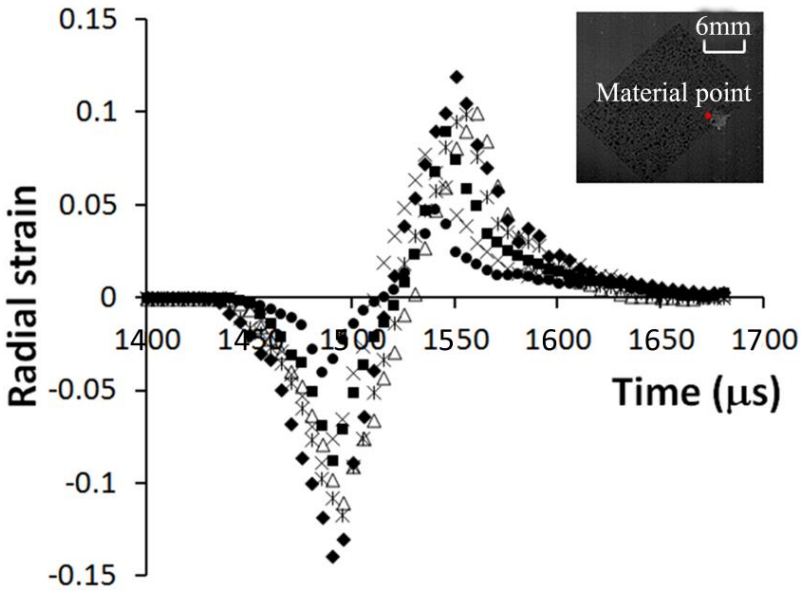

Figure 11. Inertia-driven changes in radial strain in the hydrogel during bubble growth and collapse, five typical experiments are shown. The nearest hydrogel point (in red) to the seed bubble that was not covered by growing bubble was selected. Gas seed bubbles (< 50 μm diameter) were placed to the side of the agarose hydrogel (~ 1 mm gap distance). t=0 corresponds to the start of the PSHPB experiment.

5.3.2.2 Hydrogel deformation: Single bubble underneath a tissue slice

To better capture the effects of local shock wave generated with bubble collapse, a single seed bubble was placed underneath the hydrogel slice to provide more continuous contact with the tissue surrogate during the simulated blast. Figure 12 shows a series of high speed images for a typical experiment of bubble growth (b-c) and collapse (d-e) on the left side of each image, and the calculated strain field in the hydrogel at that moment on the right side of each image.

During bubble growth, radial strains at the bubble edge are compressive. Circumferential strains at the bubble edge are tensile. Following collapse, highly localized compressive deformation resulted in maximum strain values (ε_{VM} ranged from 0.21 to 0.51) over a short duration (<24 μs) at the location of the bubble center. These strains are also larger than those determined during maximum bubble expansion. Strains are also much larger than during passage of the compressive 1D overpressure wave only (below detectable strain limit). Comparing with the previous test bubble configuration (edge placement, Figures 10 and 11), these localized shock strains are also slightly larger but over a shorter time period, see strain summary in Table 2.

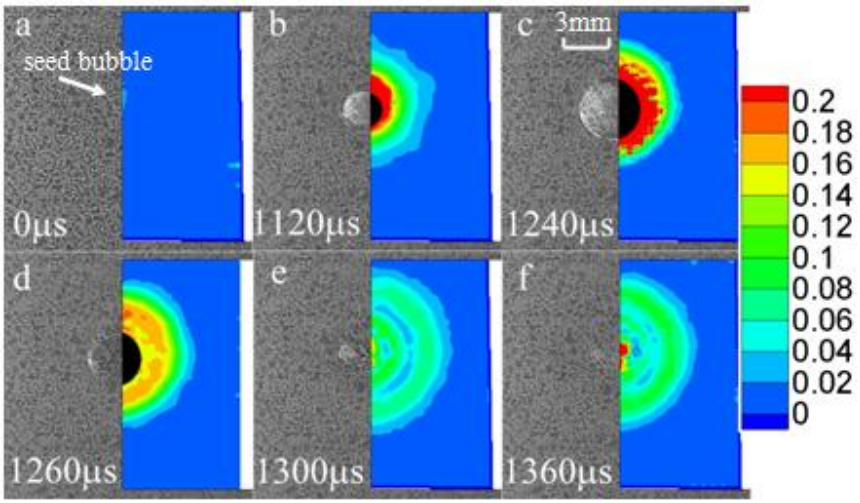

Figure 12. Typical hydrogel deformation behavior for bubble cavitation underneath a speckled hydrogel slice. (Left image) high speed images showing bubble growth (b & c) and collapse (d & e) at select time intervals; (Right image) von Mises strain maps calculated using DIC. The dark region corresponds to the bubble overlap which causes distortion in the image and so no strains were calculated in this region. Large compressive strains greater than 0.2 are measured due to localized shock waves at the bubble center after collapse (f).

Table 2. Summary of cavitation and hydrogel slice test parameters.

Group (size)	Edge placement (n=6)	Underneath placement (n=7)
Air gun pressure (kPa)	207	207
$P_{o\ max}$ (kPa)	1100±113	1088±86
$P_{u\ min}$ (kPa)	-207±32	-223±49
Lag time (□s)	61±7	53±6
Maximum *R* (mm)	2.35±0.34	2.54±0.63
P_c (kPa)	$116.3x10^3$±8.78 $x10^3$	129.1 $x10^3$±12.2 $x10^3$
$P_c/P_{o\ max}$	105.7±1.23	118.7±1.8
Maximum* ε_{rr} with bubble expansion	-0.15±0.03	-0.23±0.06
Maximum ε_{rr} inertially-driven tension	0.12±0.02	--
Maximum* $\varepsilon_{\theta\theta}$ with bubble expansion	0.06±0.01	0.17±0.03
Maximum* ε_{VM} with bubble expansion	0.17±0.05	0.27±0.16
Maximum ε_{VM} after bubble collapse	--	0.35±0.16
Local shock area † (mm^2)	--	0.18±0.03

* Maximum strain values in masked regions were not calculated; † Based on strain threshold of $\varepsilon_{VM} > 0.15$

Having characterized the single bubble test system, in the following we will present results of cavitation induced deformation and damage on live brain tissue slices. Figure 13 shows the effect of cavitation events on a rat brain tissue slice during a simulated blast with bubble initiation and growth and collapse. Note that the maximum bubble size occurs at t=1248 μs where the tissue tearing starts to occur well after the bubble has collapsed at time t = 1704 μs when localized tissue tearing was observed. These observations reveal the potential for collapse events to deform and injure soft brain tissues.

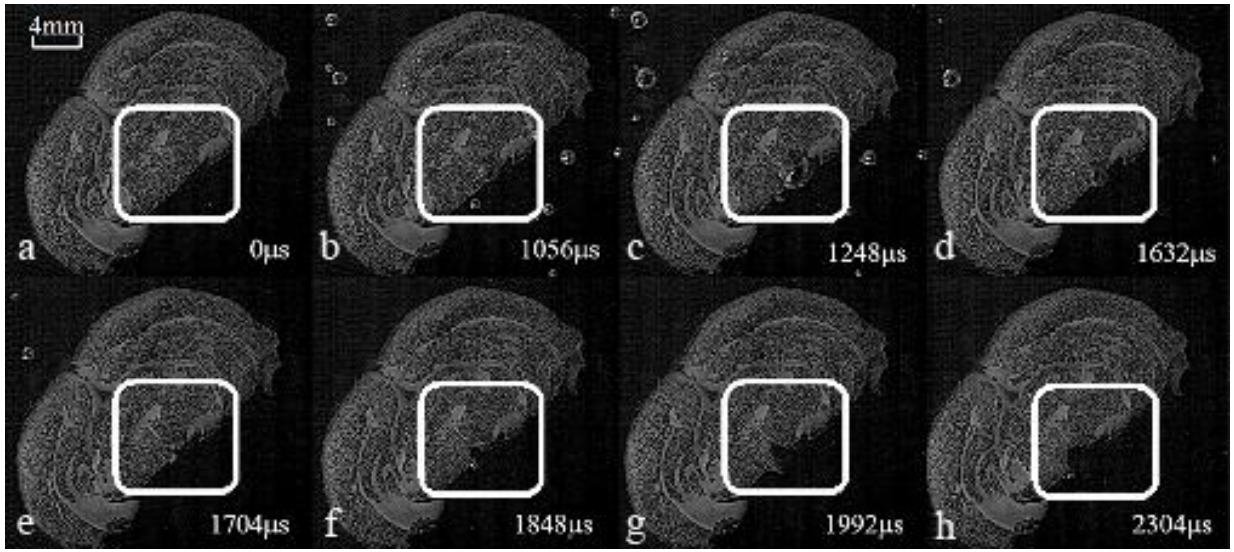

Figure 13. Effect of cavitation on a live rat brain tissue slice which was speckled and suspended in artificial cerebrospinal fluid. A simulated blast wave traveled from right to left with $P_{o\ max}$ =1045 kPa and $P_{u\ min}$= -203 kPa. PSHPB testing showed bubble initiation (b), growth (b-d) and collapse (f). Cavitation-based damage with bubble collapse was observed in the hypothalamus region (box). The tissue tearing is observed well after bubble collapse (f-h).

5.4 Early injury response due to blast and cavitation events

5.4.1 Injury due to blast wave and cavitation: High pressure test

The intent of this study was to establish characterize and analyze the progression of neural damage occurring during initial hours after exposure to high blast pressure magnitudes. The *ex vivo* model utilized acute rat brain tissue slices that were attached to a ballistic gelatin substrate and submerged in oxygenated artificial cerebrospinal fluid (aCSF). The system combined technologies of PSHPB, high-speed imaging, and histological methods to provide a controllable testing environment. The profile of pressure generated inside the chamber is graphically represented below (Figure 14). The pressure profile comprised of both underpressure and overpressure components and both formation, growth and collapse of bubbles for the duration of the test was observed. In this study, average peak fluid pressure within the test chamber reached a value of 1584±63.3 psi (Figure 14). Cavitation due to a trailing underpressure wave was also observed.

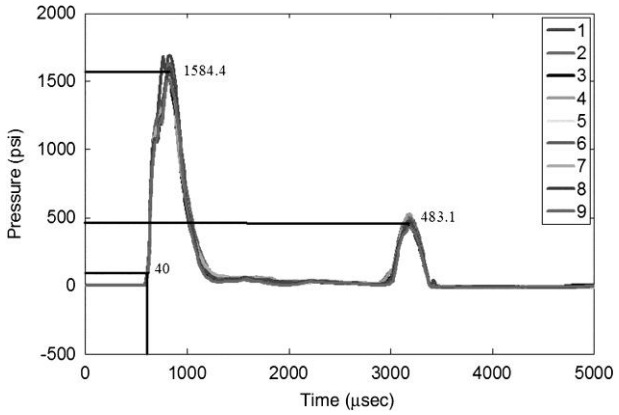

Figure 14. Artificial cerebrospinal fluid (aCSF) pressure profiles during polymer split Hopkinson pressure bar (PSHPB) testing. Profiles from 9 tests are overlaid. Average peak pressure was 1584.4±63.3 psi (±1 standard deviation), with an average full width half maximum value of 314 μsec. Pressure exceeded the trigger pressure (40 psi) at 650 μsec. Pressure waves were also reflected back along the incident bar, resulting in additional smaller impacts whose effect is assumed to be negligible compared to the 1st impact pressure. The average peak pressure of the second wave was 483.1±30.6 psi with an average full width half maximum value of 242 μsec.

Strain maps were derived from digital video images captured by the high speed camera during PSHPB testing. Normal and shear strains within the brain slices were calculated at every pixel of the brain tissue images using digital image correlation method. Time-resolved images of tissue deformation were collected and large maximum Eigen strains (0.03–0.42), minimum Eigen strains (−0.33 to −0.03), maximum shear strains (0.09–0.45), and strain rates (8.4×10^3/sec) were estimated using digital image correlation (DIC), see Figure 15.

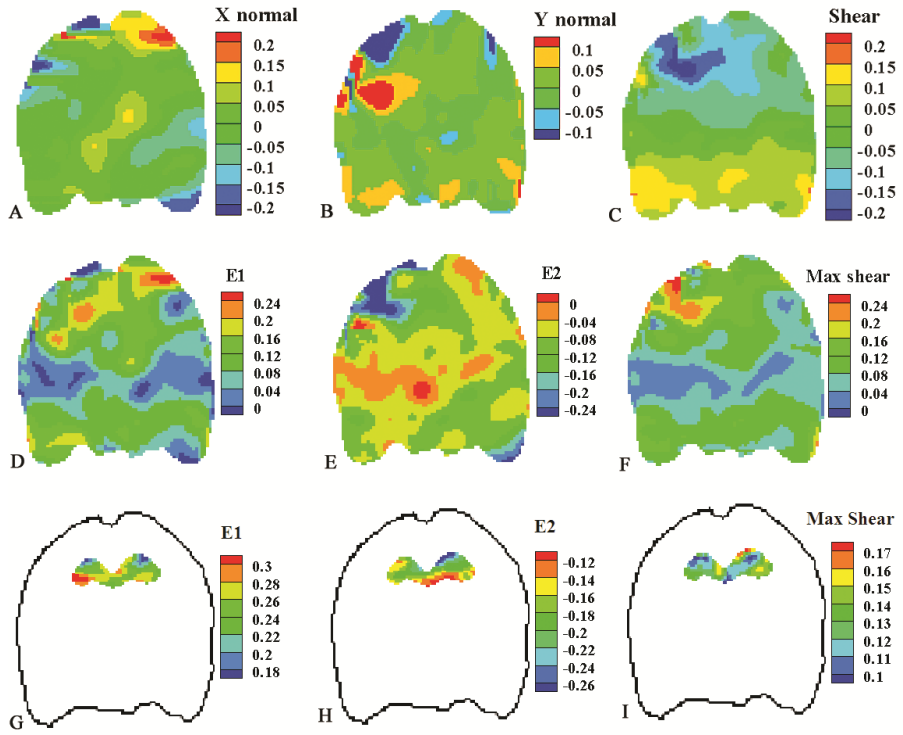

Figure 15. Strain maps of the brain. The hippocampus in this is shown separately in G-I. E1 and E2 are the maximum and minimum Eigen strains, respectively.

Neuronal injury was analyzed using a modified histological stain for degenerating neurons (Fluoro-Jade C, FJC). The protocol required to obtain the slices subjects the brain tissue to conditions of hypoxia, mechanical damage and injury. In order to obtain a timeline for mechanical testing and to determine baseline damage due to slicing protocol, effects of cell viability and tissue integrity on changes of mechanical properties of normal rat brain tissue slices were also investigated (Lee et al. 2012). Figure 16 depicts the detection timeline and sensitivity of FJC for shorter time duration following mechanical damage. Neuronal degeneration was effectively detected after 4 hours post slicing and tissue degradation was detected at 2 hours incubation time.

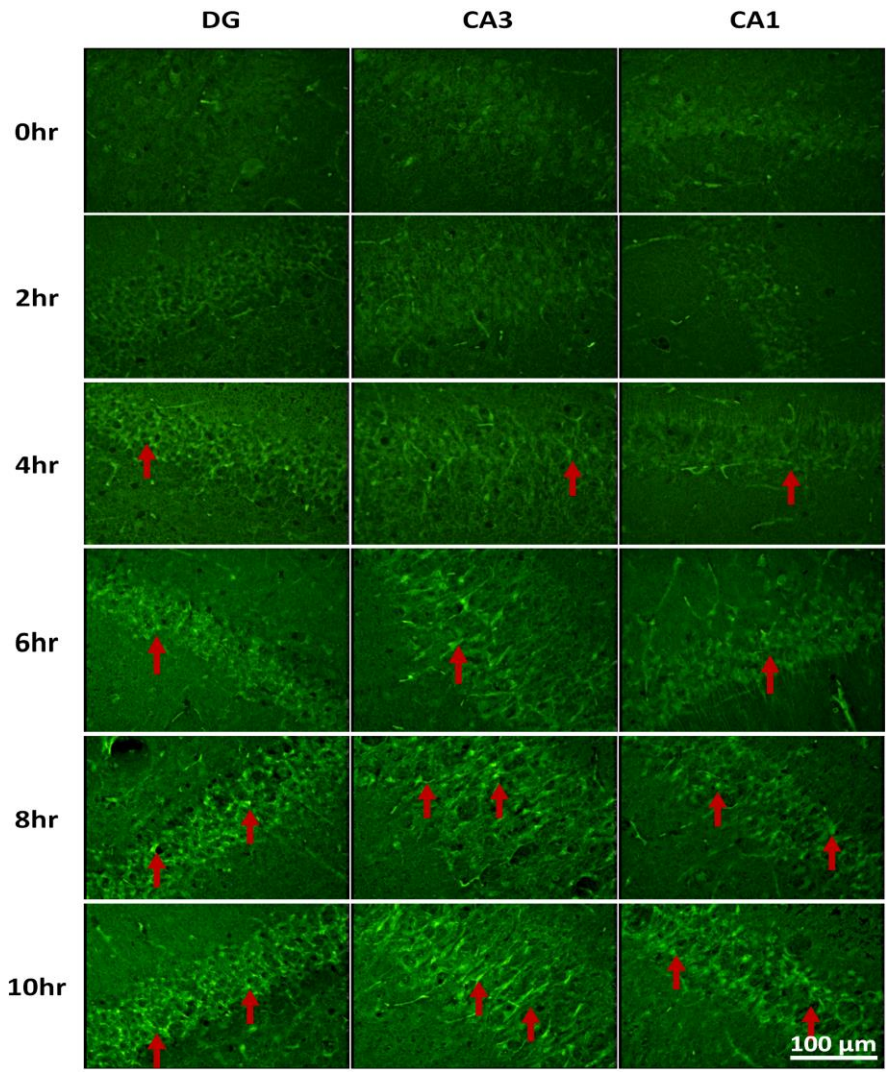

Figure 16. Viability testing of acute rat brain tissue slices. Hippocampal regions (DG: dentate gyrus, CA3 and CA1) were tested over 2 hour intervals (a- 0 hour, b- 2 hours, c- 4 hours, d- 6 hours and e-10 hours incubation time). Fluorescent images show bright green regions (red arrows) corresponding to degenerating neurons (FJC-positive). Extensive degeneration throughout the hippocampus was observed after 6 hours incubation.

Neuronal injury at 4 and 6 h after shock wave exposure in a brain tissue was quantified using Fluoro-Jade C. The total number of nuclei in the same region of hippocampus was also detected using DAPI staining. Quantitative cell counting methodology was applied to measure differences between blast exposed and control specimens between the three distinct region of the hippocampus (DG, CA1 and CA3). The result, expressed as percentage degenerating neurons was calculated for each tissue section and sub region to assess cell type and tissue spatial vulnerability, see Figure 17. Statistical analyses using General Linear Models (SAS) was conducted to examine any statistical difference between users and between control and blast exposed samples. Neuronal injury due to PSHPB testing was found to be significantly greater than injury associated with the tissue slice paradigm alone (Figure 18).

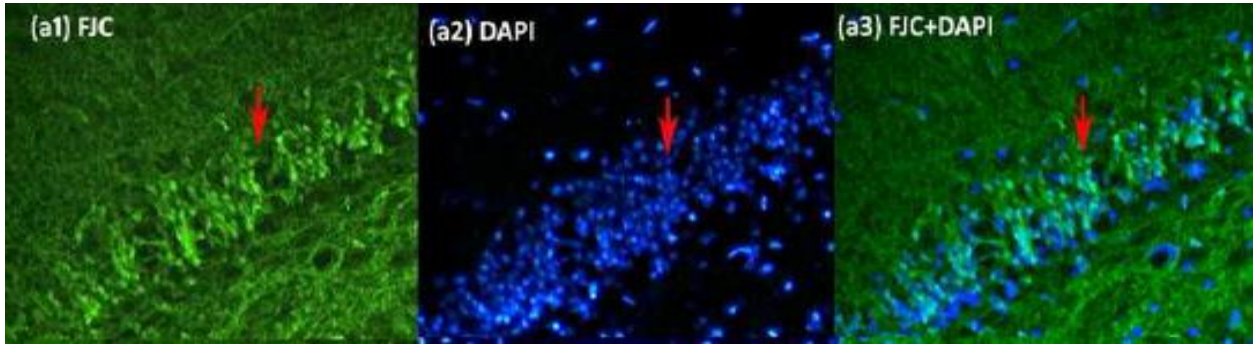

Figure 17. 4′,6-Diamidino-2-phenylindole (DAPI) and Fluoro-Jade C (FJC) image analysis within CA1. (a1) FJC-positive areas were used to identify degenerating neurons within CA1 (a2) DAPI-positive areas were used to identify the total number of nuclei within CA1 (a3) Superimposition of FJC images with DAPI images to yield the % neuronal degradation within CA1.

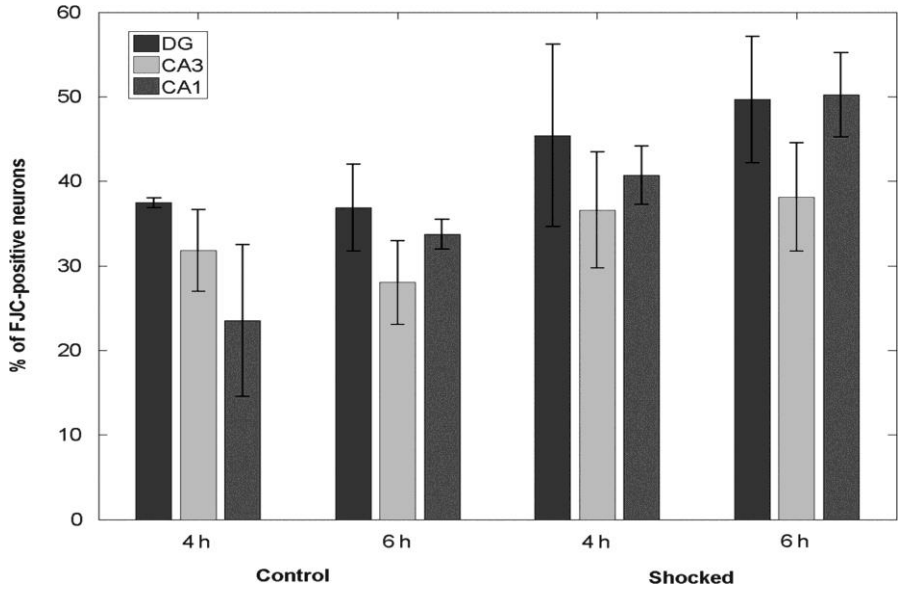

Figure 18. Neuronal degeneration in the hippocampus within control and polymer split Hopkinson pressure bar (PSHPB) test slices measured with Fluoro-Jade C and 4′,6-diamidino-2-phenylindole (DAPI) staining. Dentate gyrus (DG), CA3, and CA1 regions of the hippocampus were tested, and control and PSHPB were compared at 4- and 6-h incubation times. Significant differences in neural degeneration were measured between the control and PSHPB groups by analysis of variance (ANOVA) testing for 4 and 6 h of incubation after testing. For the 4-h incubation time, 4 brain tissue slices were used in PSHPB tests and 2 slices were used in control tests, and 72 FJC images were analyzed to estimate the fraction of neuronal degeneration. For the 6-h incubation time, 8 brain tissue slices were tested with the PSHPB, 4 slices were used for controls, and 136 FJC images were analyzed. FJC intensities higher than 30% of background intensity were considered as FJC-positive neurons. Bars correspond to 1 SD (285×226 mm, 96×96 dpi).

5.4.2 Injury due to overpressure: Low pressure test

The overpressure component of the primary blast wave is considered to be potentially damaging to the brain. Damage to astrocytes, the non- neuronal cells that are implicated in neuronal metabolic maintenance, blood–brain barrier, regulation of homeostatic environment and tissue remodeling, via direct transient physical forces has the potential to disrupt local and global functioning of neuronal tissue. In this study, the hypothesis that simulated blast shock wave overpressures, transmitted through intact but isolated brain architecture, is capable of acute astrocyte injury at early time points was studied. The temporal and energetic profile of blast waves used in this study

simulated actual blast events but did not contain underpressure components. A controlled lower peak pressure (~60psi, 1-2ms) was introduced without the characteristic negative component of the wave (Figure 19).

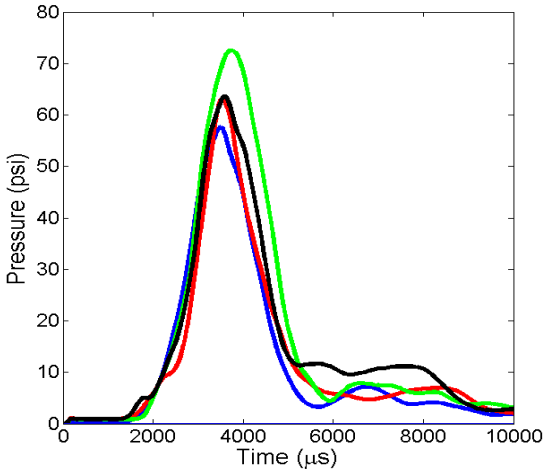

Figure 19. Test chamber pressure profiles during exposure to simulated blast via PSHPB testing. Average peak pressure inside the chamber was 60.25 ± 4.99 psi. The average full width at half maximum was 362 μs. The system allowed for a single peak loading along with absence of underpressure (negative pressure component).

Based on observation from clinical symptoms implicating the hippocampus as a blast-susceptible region, injury assessment for astrocytes was carried out in the CA1 sub-region of the hippocampus using astrocyte specific cytoskeletal protein, GFAP immunolabeling. Figure 20, highlights the morphology of astrocytes following slicing protocol. The GFAP stain revealed normal structural features like extensive detailed branching along with typical star shaped cell body.

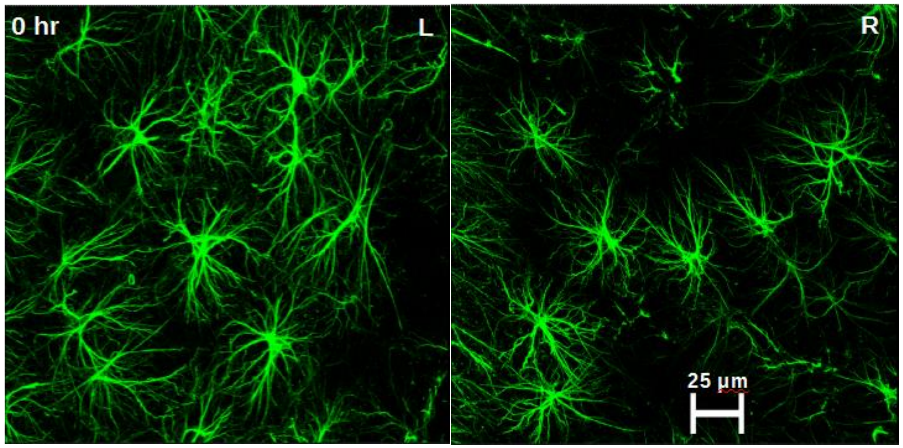

Figure 20. Baseline morphological features of astrocytes with GFAP labeling.Control slices were subjected to similar testing conditions as that of blast exposed slices without actual exposure to the blast wave or incubation. The imaging was restricted to the CA1 subregion of both hippocampi (R= right & L = left) for a given slice. At 0 hr incubation, morphology of the astrocytes appears normal.

Evolving astrocyte pathology emerges during the initial hours after exposure to overpressure alone, at magnitudes and durations comparable to real blast waves (Figure 21). Two distinct astrocyte injury profiles were identified: (a) a process similar in one respect to conventional astrogliosis, with an increase in GFAP immunoreactivity in GFAP-positive cells, and (b) a process comparable to clasmatodendrosis, an acute autolytic phenomenon, characterized by voids in cytoplasm in conjunction with rounded somata and disintegrating processes. The latter has not been previously associated with blast-induced injury, and neither has been previously demonstrated as acute responses reflecting distinct astrocyte vulnerability.

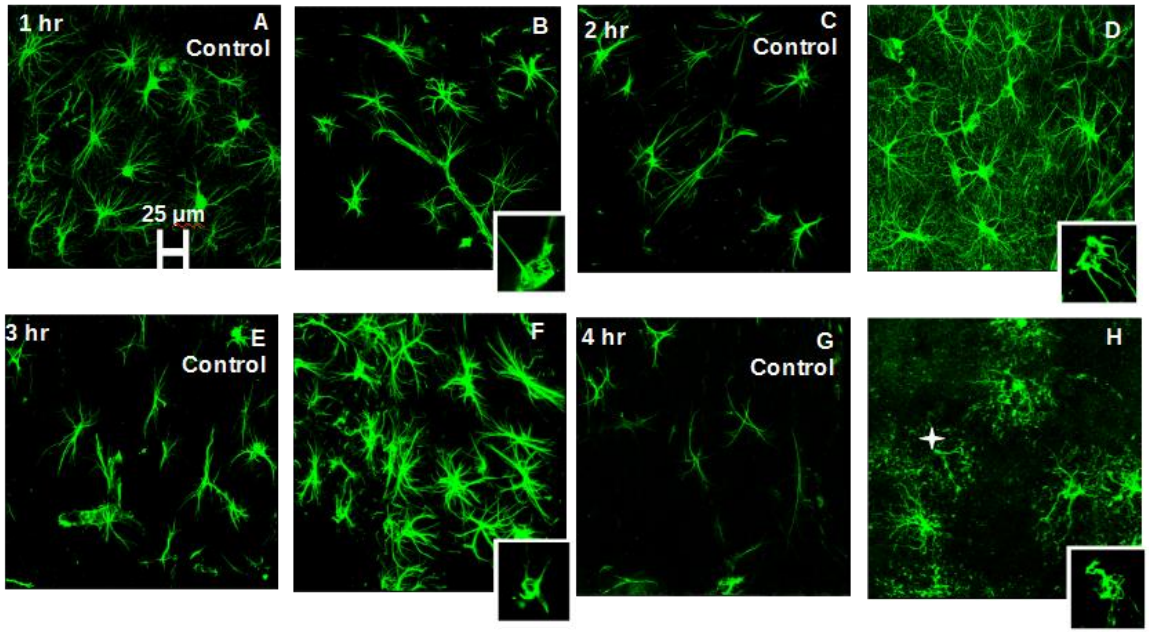

Figure 21. GFAP immunolabeled hippocampal astrocytes from control (left) and blast- exposed slices (right) as a function of post-exposure incubation time. At 1 hr. incubation time the morphological features from control (A) and blast exposed (B) look similar with the stellate shape and radial extension. At 2 hr. incubation qualitative visual differences can be seen between control (C) and blast exposed (D) astrocytes. Blast-exposed astrocytes appear hypertrophied and show enhanced GFAP staining of the cell bodies along with increased background staining of fine processes. After 3 hr. incubation, blast-exposed astrocytes (F) showed enhanced GFAP staining when compared to control slices (E). At 4 hr. incubation, clasmatodendritic features were observed in astrocytes from the blast-exposed slices (H) when compared to control slices (G). Astrocytes from control slices (G) showed reduced complexity of processes. Astrocytes from the blast-exposed slices (H) showed beaded, presumably disintegrating processes (star). Insert figures highlight are individual confocal planes highlighting GFAP negative voids in the cytoplasm along with rounded appearance of somata.

Immunofluorescent GFAP distribution and intensity were analyzed across treatment groups during initial hours after the blast exposure. The area fraction occupied by GFAP positive cells and the intensity of the GFAP within these areas were quantified using Fiji (NIH Image). Contributions to overall variance were tested using a general linear model (SAS Proc GLM) for the potential effects of shock, incubation time, brain hemisphere, image fields (within-slice), slices (within-animal), and interactions.

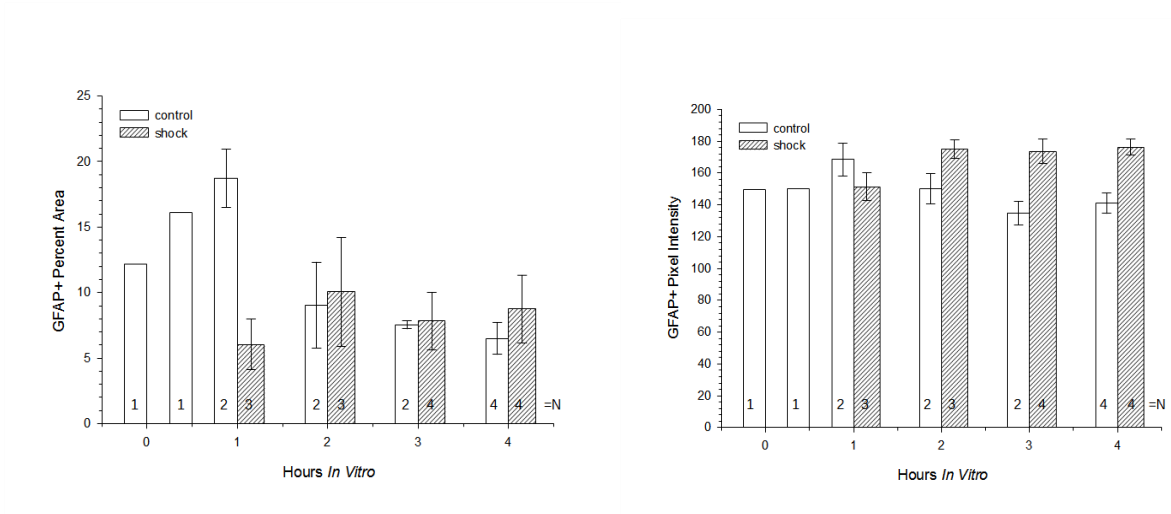

Figure 22. Area fraction of GFAP immunoreactivity and average GFAP intensity between treatment conditions over the incubation time points tested. Mean ± s.e.m. area fraction of GFAP immunoreactivity and average GFAP intensity as a function of incubation time. N within the bars indicates the slices used to collect the data. Each slice contributed to an average of 25 image fields. Main effects and interactions were tested in a general linear model (SAS Proc GLM). With the exception of 1 hr. incubation time, the GFAP immunoreactivity in astrocytes was significantly higher than control at all time points. The area fraction was found to be not affected by blast, time, brain side, or slice within animal. Asterisk, $p < 0.05$ compared to control slices from same time point.

5.4.3 Injury due to cavitation: Controlled single bubble test

The intent of this study is to evaluate the morphological and histological changes that are induced due to cavitation events. The methodology developed for the controlled single bubble test is extended to study damage induced by cavitation on acute brain tissue slices. The pressure profile used in these test consisted of both overpressure and underpressure components (Figure 23).

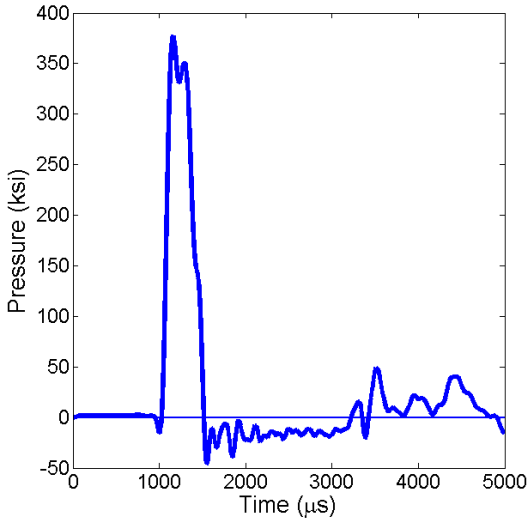

Figure 23. Pressure profile of the input simulated blast wave with both overpressure and underpressure components.

The region of interest was focused on the hippocampus and in these preliminary tests; the bubble was placed under the hippocampal region. Upon bubble growth and collapse, large deformation of one side of hippocampus was visible from the high speed images long after the bubble collapse (Figure 24).

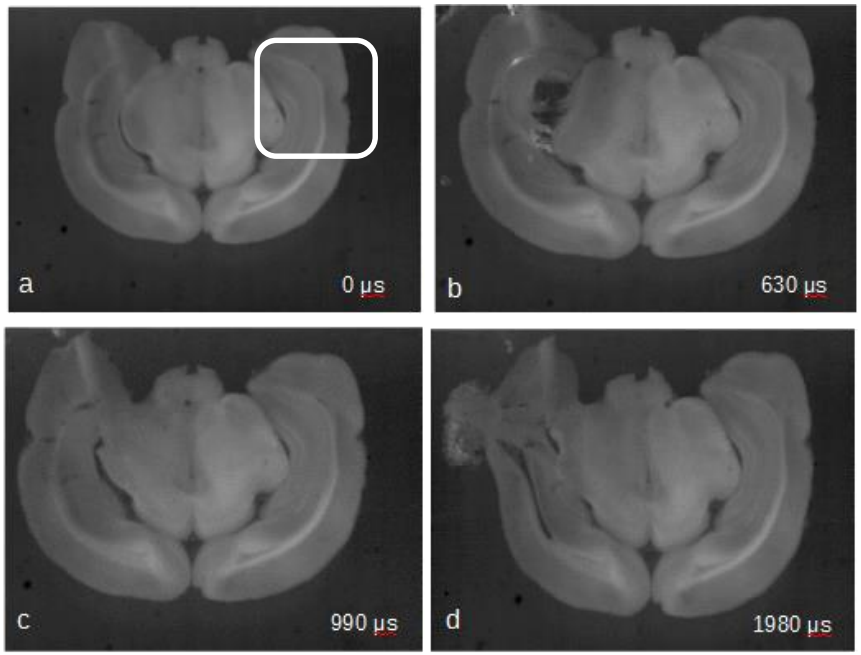

Figure 24. Sequential images of the bubble growth and collapse. (a) start of bubble growth (b)the rectangular space indicates the bubble at its maximum size (c) initial bubble collapse, and (d) brain tissue deformation after large time following bubble collapse.

Upon subsequent SEM imaging, qualitative differences were observed between the two hippocampi on the same slice. The hippocampal side directly influenced by the bubble (right), showed a visible surface gap in the DG layer when compared to the left side. Observing the surface under high magnification, long continuous processes were observed on the left side (Figure 25). At the equivalent location on the right side, the processes appeared to be broken and a large gap was observed.

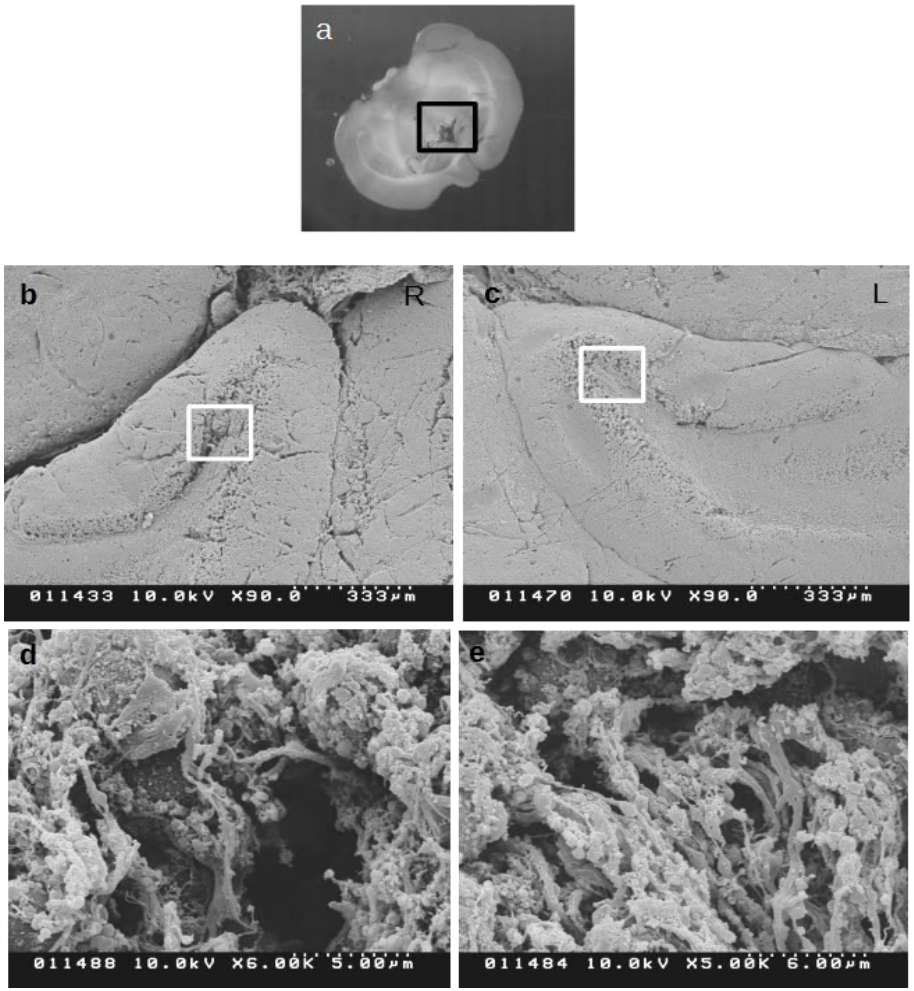

Figure 25. Scanning electron microscope images of hippocampus subjected to cavitation. (a) The brain tissue slice deformation during the maximum bubble size, with the black rectangle highlighting the bubble placement. (b) Large field view of the right hippocampus that was directly impacted by the bubble growth and collapse. A fractured surface is evident in the DG layer. (c) Large field view of the left hippocampus. The surface appears clean without any visible damage. (d) Magnified view of the white rectangular area from image (a). A large gap is evident in the center. (e) Magnified view of the white rectangular area from image (b). Long continuous processes are visible.

5.5 Brain tissue mechanical properties

During blast induced TBI, brain tissue potentially undergoes complex motions such as compression, tension, shear and torsion which can cause axonal disconnection and distortion, necrotic cell damage and intracerebral hemorrhage. These damages can lead to changes in physical structure and in turn affect the mechanical properties of the brain. However, in heterogeneous tissues like the brain, there are limitations to using homogenous assumptions when explaining complex tissue interactions between different anatomical regions. There is a need for additional measures of spatial as well as transient variation in mechanical properties within different anatomical regions of the brain. Viscoelastic properties are useful for describing transient mechanical behavior and corresponding modulus values can vary with time scale. Thus, knowledge of mechanical properties of brain tissue is important in characterizing structural changes with injury in addition to analyzing internal stresses with deformation.

Optical coherence tomography (OCT) is a bioimaging technique that utilizes low coherence interferometry to measure the back scattered light reflected from the sample to generate cross sectional images. It is noninvasive and provides real time imaging of biological samples at micrometer scale. In first–of–a-kind experiments we have combined OCT with micro-indentation to measure the mechanical properties of brain tissue slices. This set up allows us to test over long creep testing times when compared to other test systems. We have used this system to measure mechanical as well as optical properties within different brain regions including cerebral cortex, putamen, hippocampus, thalamus, and corpus callosum were measured. Indentation creep tests determined viscoelastic properties of ex vivo rat brain tissue slices in different anatomical regions (Figure 26).

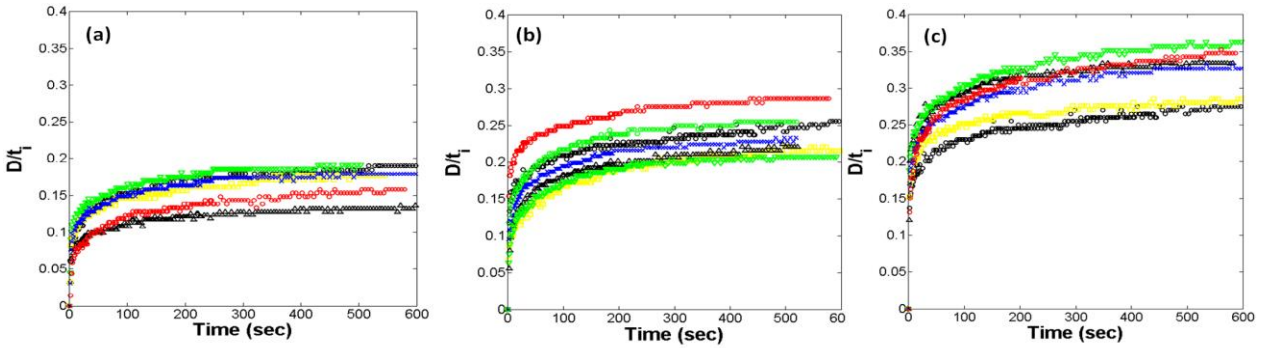

Figure 26. Normalized creep indentation in the (a) rat cerebral cortex, (b) hippocampus, and (c) caudate/putamen over 10 min. Deformation depth ratio was the ratio between undeformed and deformed tissue thickness. *n*=6 for cerebral cortex and putamen and *n*=7 for hippocampus. Data clustering was the result of discretization introduced by limited vertical resolution (1 pixel = 1.37μm).

The viscoelastic parameters and relaxation of shear modulus were estimated by fitting to an isotropic neo-Hookean model. The average equilibrium shear modulus for normal brain was estimated as 0.2 kPa in hippocampus region, 0.45 kPa in the cerebral cortex and 0.11 kPa in the caudate-putamen see Figure 27. Differences in the shear modulus decay across different anatomical region in the brain can be attributed to the morphological and mechanical heterogeneity. Even gray regions between different anatomical regions showed different viscoelastic properties. This can be accounted for due to differences in size, density and structure between the anatomical regions.

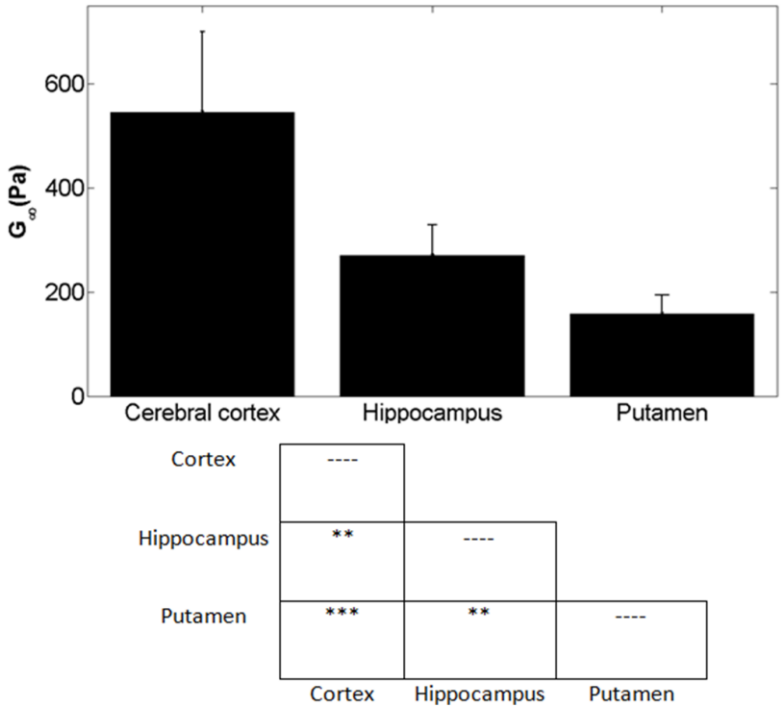

Figure 27. Estimated equilibrium shear modulus in three different anatomical regions of brain tissue slices. ANOVA tests showed significant differences in shear moduli between the cortex, hippocampus and caudate/putamen. Statistical analysis was performed using SAS. For α =0.05, *** p-value <0.0002, **p-value<0.002. Bars show ± 1SE.

Effects of cell viability and tissue integrity on changes of mechanical properties of normal rat brain tissue slices were also investigated. Propidium Iodide (PI), FluoroJade C (FJC), DAPI and Hoechst assays were utilized to detect and changes in cell viability and degradation, see Figure 16 & 28. The PI stains were able to detect early necrotic cell death following tissue slicing. PI stain labeled the dead/ damaged neuronal cells while Hoechst stain stained all the cell bodies in a given region. Figure 28 shows a comparison of PI and Hoechst stains for hippocampus region of a normal rat brain. Most necrotic cell damage was detected 20 μm below tissue surface indicating damage due to slicing. These results provided a suitable time line for in vitro mechanical testing.

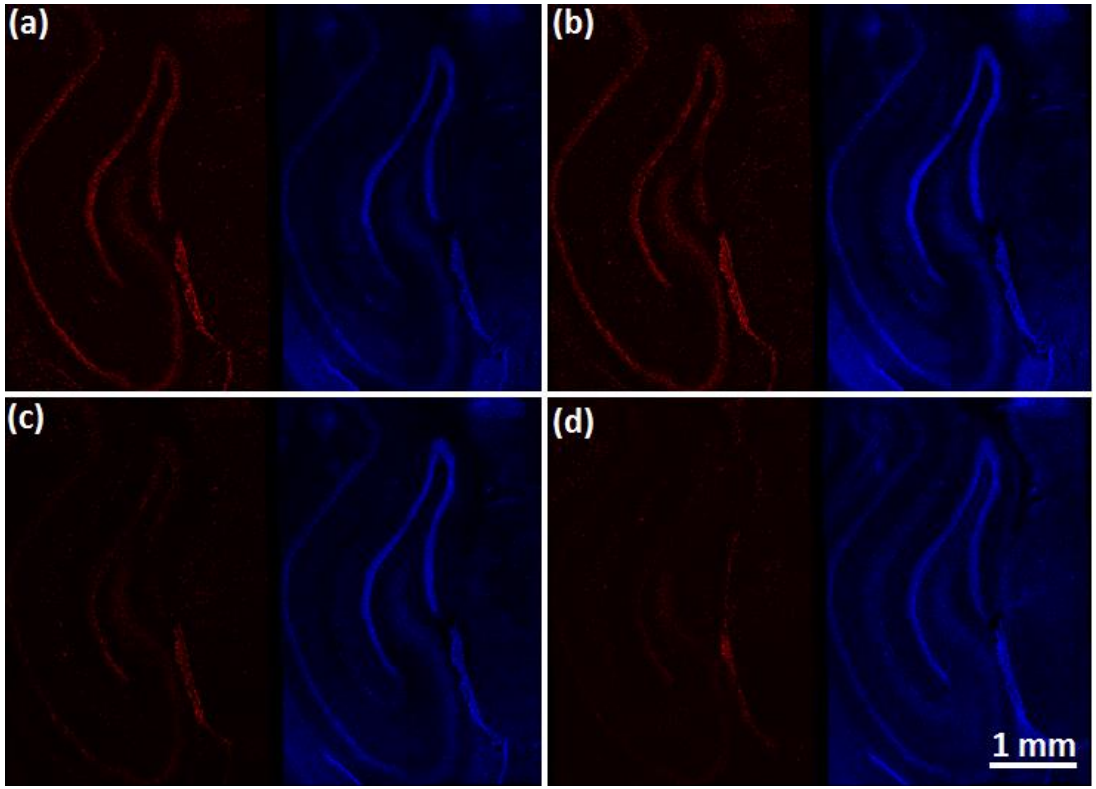

Figure 28. Necrotic cell death in the hippocampus of acute brain tissue slices after slicing. PI staining (red fluorescence) labeled damaged and dead cells. Hoechst (blue fluorescence) labeled the total cells in the same field of view. Confocal images obtained at 10x magnification and 10 μm depth intervals. (a) Surface of tissue slice, (b) 10 μm, (c) 20 μm, and (d) 40 μm depths below the surface of the tissue slice.

V. Technology Transfer

Discussions were held 2010 at the Society of Biomedical Engineering (SBE) conference with Dr. Reuben Kraft on high rate induced deformation characteristics in gels

Worked directly with Dr. David Moore (Defense and Veterans and Brain Injury Center) to create brain model conditions of clinical relevance.

The PI gave a seminar at ARL on 28 May 2014 titled "Cavitation Induced Damage in Brain Tissue: Relevance to TBI". Around 40 researchers attended the seminar. Separate discussions were held with Drs. Sikhanda Satapathy and Christopher Hoppel and others in the group. Manuscripts of the relevant materials were also sent to ARL for distribution among interested researchers. Discussions were held to identify specific areas of interest to ARL so that research can continue for mutual benefit.

Most recently, the PI met with Dr. Rohan J Banton of ARL who also expressed interest in the papers. The PI has sent those papers as well.

The PI has presented his research at numerous conferences where ARL researchers such as Dr. Tusit Weerasoorya have attended the sessions and have interacted with the PI. His post-doc also attended the seminar at ARL and it is his understanding that she is working on developing similar experimental techniques for shock loading of soft tissue.

VI. Journal Articles

Papers:

Hong, Y., Sarntinoranont, M., Canchi, S., King, M.A., Subhash, S., "Localized Tissue Surrogate Deformation due to Controlled Single Bubble Cavitation," *Submitted to Soft Matter.*

Canchi, S., Sarntinoranont, M., Hong, Y., Subhash, S., King, M.A., "Simulated Blast Overpressure Induces Specific Astrocyte Injury in an Acute Brain Slice Model," *Submitted to J. Neurotrauma.*

Lee, S.J., King, M.A., Sun, J., Xie, H.K., Subhash, G., Sarntinoranont, M. "Measurement of Viscoelastic Properties in Multiple Anatomical Regions of Acute Rat Brain Tissue Slices," *Journal of the Mechanical Behavior of Biomedical Materials*, 29: 213-224, 2014.

Sarntinoranont, M., Lee, S.J , Kwon, J., Hong, Y., King, M.A., Moore, D.F., Subhash, G., "Blast-Induced Traumatic Brain Injury Model using Submerged Acute Rat Brain Tissue Slices," *Journal of Neurotrauma*, 29(2), 418-429, 2012.

Sun, J., Lee, S.J., Wu, L., Sarntinoranont, M., Xie, H., "Refractive Index Measurement of Acute Rat Brain Tissue Slices using Optical Coherence Tomography," *Optics Express*, 20(2): 1084-1095,2012.

Lee, S.J., Sun, J., Flint, J.J., Guo, S., Xie, H.K., King, M.A., and Sarntinoranont, M., "Optically Based-Indentation Technique for Acute Rat Brain Tissue Slices and Thin Biomaterials" *Journal of Biomedical Materials Research: Part B*, 97B (1):84-95, 2011

Conference Abstracts and Presentations:

"Cavitation Induced Damage in Brain Tissue: Relevance to TBI", Army Research Laboratories, Aberdeen Proving Ground, 28 May 2014

Canchi, S., Hong, Y, Flint, J., Sarntinoranont, M., Subhash G., King, M.A. "Simulated Blast Overpressure-Induced Astrocyte Injury in an Acute Brain Slice Model," *Neuroscience 2014*, Washington, DC, November 15-19, 2014.

Canchi, S., King, M.A., Sarntinoranont, M., Subhash G.,., "Immunohistochemical Study of Astrocytes following Blast-Induced Traumatic Brain Injury: A Model Study using Submerged Acute Rat Brain Tissue Slices in a Pressure Chamber," *31st Annual National Neurotrauma Symposium*, Nashville, TN, August 4-7, 2013.

Canchi, S. , Hong, Y. , Lee, S.J. , Sarntinoranont, M., Subhash, G. , King, M.A., "Optically-based Indentation for Brain Tissue: A New Histological Approach," *36th Annual American Society of Biomechanics Meeting*, Gainesville, FL, August 15-18, 2012.

Hong, Y., Canchi, S., King, M.A., Lee, S.J., Sarntinoranont, M., Subhash, G. , "Development of a test system to study brain tissue damage due to cavitation," *36th Annual American Society of Biomechanics Meeting*, Gainesville, FL, August 15-18, 2012 , 2 pages

Lee, S.J., Sun, J., King, M., Xie, H., Sarntinoranont, M., "Viscoelastic Property Changes of Acute Rat Brain Tissue Slices as a Function of Cell Viability," Proceedings of the ASME 2011 Summer Bioengineering Conference, Farmington, PA, June 22-25, 2011, SBC2011-53909 (2 pages).

Subhash, G., "A Technique for Dynamic Deformation of Submerged Brain Tissue Slices" 2011 SEM Annual Conference & Exposition on Experimental &Applied Mechanics, Mohegan Sun, Uncasville, Connecticut, June 13-16, 2011.

Lee, S.J. , Hong, Y. , King, M.A., Moore, D.F., Sarntinoranont, M., Subhash, G. , "Ex Vivo Model of Blast-Induced Traumatic Brain Injury using a Polymer Split Hopkinson Bar," *Neuroscience 2011*, session 561, Washington DC, Nov 12-16, 2011.

Sarntinoranont, M. Lee, S.J., Kwon, J., Hong, Y., King, M.A., Moore, D.F., Subhash, G., "Blast-Induced Traumatic Brain Injury Model using Submerged Acute Rat Brain Tissue Slices," 2010 BMES Annual Meeting, Hartford, CT, October 12-15, 2011.

Sarntinoranont, M. Lee, S.J., Kwon, J., Hong, Y., King, M.A., Moore, D.F., Subhash, G., "High Strain-Rate Testing of Brain Tissue Slices: Blast-Induced Traumatic Brain Injury," 63rd American Academy of Neurology Annual Meeting, Honolulu, Hawaii April 9-16, 2011.

Subhash, G., Sarntinoranont, M. Lee, S.J., Hong, Y., King, M.A., "Quantification of high loading rate induced structural and neuronal damage in live brain tissue slices," 4th International Conference on the Mechanics of Biomaterials and Tissues, Waikoloa Beach, Hawaii, Dec 11-15, 1 page, 2011.

Sarntinoranont M, Lee SJ, Kwon J, Hong Y, King MA, Moore DF, Subhash G. High Strain-Rate Testing of Brain Tissue Slices: Blast-Induced Traumatic Brain Injury NEUROLOGY, 76 [9] A159-A159 Suppl. 4 (MAR 1 2011)

Lee, S.J., Sun, J., Xie, H.K., King, M.A., Sarntinoranont, M., "The Effect of Cell Viability on Mechanical Properties of Acute Rat Brain Tissue Slices," 2010 BMES Annual Meeting, Austin, TX, October 6-9, 2010.

Presentations:

Subhash, G "Traumatic Brain Injury: An Engineer's Perspective", Department of Mechanical and Aerospace Engineering, North Carolina State University, Raleigh, NC Apr 19, 2012

Sarntinoranont, M. Lee, S.J., Kwon, J., Hong, Y., King, M.A., Moore, D.F., Subhash, G., "Blast-Induced Traumatic Brain Injury Model using Submerged Acute Rat Brain Tissue Slices," 2010 BMES Annual Meeting, Hartford, CT, October 12-15, 2011.

Subhash, G., "Characterization of Soft Tissue Surrogates and Brain Tissue for Development of Pressure-Deformation-Injury Maps at High Loading Rates, "California Institute of Technology, Pasadena, CA. Apr 11, 2011.

Subhash, G., "A Technique for Dynamic Deformation of Submerged Brain Tissue Slices" 2011 SEM Annual Conference & Exposition on Experimental &Applied Mechanics, Mohegan Sun, Uncasville, Connecticut, June 13-16, 2011.

VII. Awards and Honors

'Significant Contribution Award' American Nuclear Society (ANS) - Materials Science and Technology Division (MSTD) (2014)

'Member-at-Large' Society of Experimental Mechanics Executive Board (2015-2017)

'Fellow of SEM' Society of Experimental Mechanics, for "Contributions to the field of mechanics and materials through fundamental experimental and theoretical investigations for high strain rate, multi-axial response of novel materials, including fracture under extreme environmental conditions, to increase understanding of material behavior." (2014)

'Technology Innovator Award' University of Florida *(2014)*.

'University of Florida Research Foundation Professor' University of Florida *(2013)*

'Teacher/Scholar of the Year' College of Engineeirng, University of Florida (2013)

'Researcher of the Year' Mechanical and Aerospace Engineering Department, University of Florida (2011)

VIII. Graduate Students Involved Directly in ARO Project

Sung, Jin Lee, Ph.D. – He has graduated

Yu Hong, Ph.D. - He has graduated

Saranya Canchi - She is a current Ph.D. candidate (Expected to graduate in Spring 2015)

Cavitation-Induced Structural and Neural Damage in Live Brain Tissue Slices: Relevance to TBI

Ghatu Subhash, University of Florida, 36 mo. (+12 mo. NCE), FY10-FY14, ARO Core Program, $392K

Objective: Quantify cavitation conditions within the cerebrospinal fluid (CSF) and develop 'pressure-deformation-injury' maps for brain slices.

Scientific Challenges: 1. Pathogenesis of b-TBI following blast exposure is not well understood.

2. Neuroimaging techniques for detection of cavitation induced injury do not exist.

3. Experimental platforms to visualize and resolve real-time incidence of cavitation and tissue deformation following blast exposure are unavailable.

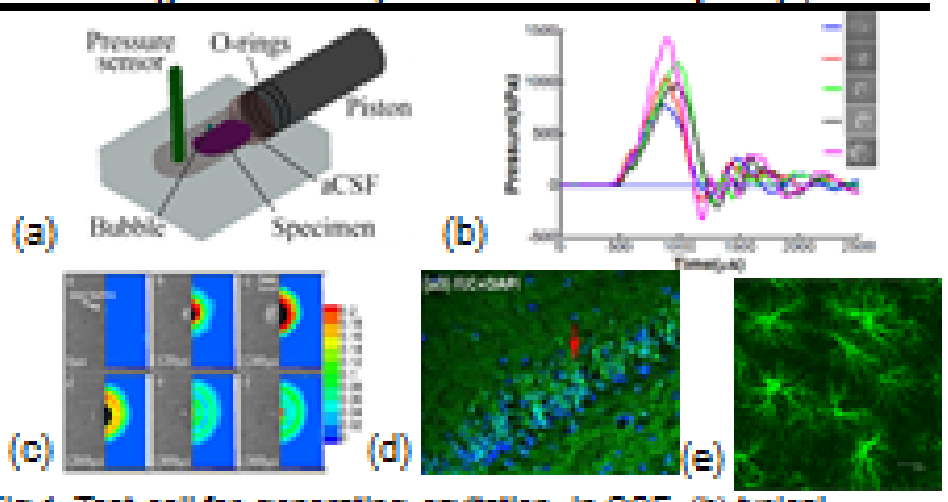

Fig.1. Test cell for generating cavitation in CSF, (b) typical pressure pulse and maximum bubble size, (c) Strain in a gel slice during cavitation, revealing large strain after bubble collapse, (d) degenerating neurons (green) and total cells (blue) in Hyppocampus and (e) astrocyte degeneration following shock.

Major Accomplishments:

1. Establishment and characterization of controlled single bubble cavitation following blast exposure.

2. Spatial mapping of deformation and strain on tissue surrogates following cavitation.

3. Identification of temporal progression of neural and astrocyte pathology following blast exposure.

Personnel: 2 faculty, 1 research scientist, and 3 graduate students (2 graduated and 1 in progress).

Army Relevance: Identification of injury mechanisms may result in novel mitigation strategies, e.g. protective gear or improved drug therapies specific to this injury.

Funding profile: FY10 $64K; FY11 $$130K; FY12 $134K; FY13 $ 64K

Grant # W911NF-10-1-0276

PI Contact information: Subhash Ghatu
Ph: 352-392-7005
Fax 352-392-7303
Email: subhash@ufl.edu